# Liquefaction in Palu: The Cause of Massive Mudflows

**Abdul Jalil** ( abduljalil@mail.ugm.ac.id )
Department of Civil Engineering, Faculty of Engineering, Universitas Malikussaleh, Aceh 24355, Indonesia

**Teuku Faisal Fathani**
Universitas Gadjah Mada Fakultas Teknik

**Iman Satyarno**
Universitas Gadjah Mada Fakultas Teknik

**Wahyu Wilopo**
Universitas Gadjah Mada Fakultas Teknik

**Research**

**Keywords:** Liquefaction potential, Microtremor, HVSR, Ground shear strain, Mudflow

**Posted Date:** January 6th, 2021

**DOI:** https://doi.org/10.21203/rs.3.rs-137316/v1

# Liquefaction in Palu: The Cause of Massive Mudflows

Abdul Jalil[1,4,*], Teuku Faisal Fathani[1,3], Iman Satyarno[1,3] and Wahyu Wilopo[2,3]

[1] Department of Civil and Environmental Engineering, Faculty of Engineering, Universitas Gadjah Mada, Yogyakarta 55281, Indonesia; abduljalil@mail.ugm.ac.id;tfathani@ugm.ac.id; imansatyarno@ugm.ac.id
[2] Department of Geological Engineering, Faculty of Engineering, Universitas Gadjah Mada, Yogyakarta 55281, Indonesia; wilopo_w@ugm.ac.id
[3] Center for Disaster Mitigation and Technological Innovation (GAMA-InaTEK), Universitas Gadjah Mada, Yogyakarta 55281, Indonesia
[4] Department of Civil Engineering, Faculty of Engineering, Universitas Malikussaleh, Aceh 24355, Indonesia

Abstract:

The 7.5 Mw tectonic earthquake that hit Palu City on 28 September 2018 was followed by tsunami and liquefaction that triggered massive mudflows in Balaroa, Petobo, and Jono Oge areas. Extensive damages to infrastructures occurred as the result of these earthquake-triggered disasters. This study explores the causing factors of the massive mudflow in Balaroa, Petobo, and Jono Oge areas as it is a quite rare phenomenon. This study focuses on the causing factors of liquefaction such as the condition of soil lithology, depth of water table, distance to the fo[1]cal mechanism, and the thickness of soft sediment. To carry out the liquefaction analysis, important data, such as microtremor data which included the Horizontal Vertical Spectral Ratio (HVSR), geological condition, and borehole data, were examines. Additional data i.e. ground layers slopes and other factors were also investigated. Normally, these data are not considered when observing common liquefaction. However, for the case of massive mudflows in Balaroa, Petobo, and Jono Oge, they become the key factors. Based on the microtremor data, the analysis results show that the distribution of ground shear strain values in Palu City ranges from $0.75\times10^{-4}$ to $2.56\times10^{-4}$. The distribution of the locations of the liquefaction corresponds to the distribution of ground shear strain values. High ground shear strain values were discovered in Palu City valley. Such high value and groundwater level indicate that liquefaction in Palu City will certainly take place. The semi-empirical method confirms that Balaroa, Petobo, and Jono Oge have high potential for large-scale liquefaction to occur at a maximum depth of 16 meters below the ground surface. Having loose soil grain with high water content, the soil will turn into a massive amount of mud during the liquefaction. In addition, ground slopes and ground vibration due to the earthquake will create massive mudflows similar to flash flood. However, the mudflows movement is slow since the slope inclination is slight.

**Keywords**: Liquefaction potential, Microtremor, HVSR, Ground shear strain, Mudflow

## Introduction

On September 28, 2018, an earthquake of Mw 7.5 struck Central Sulawesi Province, Indonesia. The earthquake hypocenter was located at a depth of 11 km and geographic coordinate of 0.18°S and 119.85°E, resulted in extensive damage (**Fig. 1**) as well as mudflows in Palu City (Valkaniotis et al. 2018; Mason et al. 2019). The mudflow covered the areas of Balaroa, Petobo and Jono Oge as shown in **Fig. 1b**, **Fig. 1c**, and **Fig. 1d**, respectively. The largest life loss due to the liquefaction in Palu could probably be attributed to the three mudflows, which moved material within hundreds of meters downslope parallelly. Two of these mudflows which originated as lateral spreads directly beneath the Gumbasa irrigation channel, occurred at Petobo, and Jono Oge (**Fig. 1c**, **d**). Meanwhile, the mudflow in Balaroa was located close to the Palu Koro fault line and was interpreted that it fell along the fault as it was close to the fault line. The mudflow left severe damages on a large part of the soil on the gentle slopes of Palu City (Socquet et al. 2019). Some of the mudflows moved within a distance of 1 km, approximately. The damaged Gumbasa irrigation channel triggered flash floods which turned into wave-like mudflows (Mason et al. 2019). Gumbasa irrigation channel was an anthropogenic hazard of unexpected landslides in Palu that clearly demonstrated the need of more proactive assessment (Bradley 2019).

The epicentral distance to the liquefaction site in Palu City was plotted in an image developed by (Ambraseys 1988) based on the database regarding shallow earthquakes around the world (**Fig. 2**). As shown in **Fig. 2**, the

* Correspondence: abduljalil@mail.ugm.ac.id
Civil and Environmental Engineering, Universitas Gadjah Mada, Yogyakarta, Indonesia.

distance between Palu City and the epicenter of the 7.5 $M_w$ earthquake was 80 km, which indicated consistency with the findings.

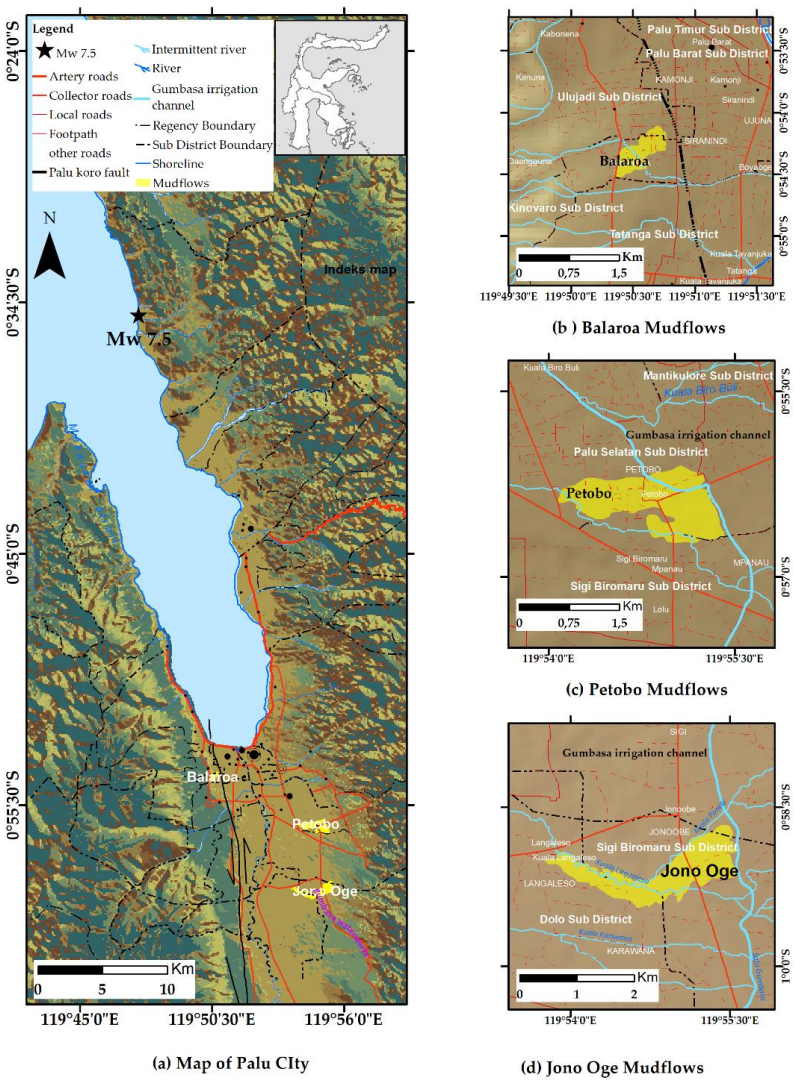


**Fig. 1** Liquefaction resulting mudflows in Palu City: (**a**) Map of Palu City, (**b**) Balaroa mudflows, (**c**) Petobo mudflows, and (**d**) Jono Oge mudflows

The Meteorological, Climatological, and Geophysical Agency (BMKG) reported that the earthquake that hit the city and coastal area caused enormous damages to the settlements and buildings (Sadly 2018). This event also resulted in liquefaction, landslide, and mudflows (Mason et al. 2019). Thus, it is required to carry out liquefaction and mudflows research to identified and reduce the disaster risk.

The Palu City Soil Investigation report conducted by (Widyaningrum 2012) in 2012 mentioned that the area was composed of alluvium deposits with sand layer at the top, silt in the middle, and clay in the bottom. (Widyaningrum 2012) also reported shallow groundwater table on the site. Research on liquefaction potential in Palu City was conducted by (Widyaningrum 2012) using the semi-empirical and index potential liquefaction (LPI) methods. Although this study provides valuable information regarding the liquefaction susceptibility in Palu area, the researchers only used semi-empirical and geological procedures, hence, the effect of liquefaction that causes mudflow was not explained in this study. In general, previous studies analyzed the liquefaction potential based on the semi-empirical approach proposed by Idriss and Boulanger (Idriss and Boulanger 2008). The liquefaction potential index (LPI) was determined by referring to the Iwasaki methods (Iwasaki et al. 1981). The National Center for Earthquake Study (Irsyam et al. 2019) released a collateral hazard map due to the 2018 earthquake in Palu, which included flow liquefaction and mudflow.

Some researches on liquefaction studies applies the microtremor wave propagation. In addition, the researchers also made numerical models of geotechnical effects of differences in seismic parameters (Araujo and Ledezma

2020). This study was carried out by correlating the wave characteristics, soil site classification, and liquefaction evidence during the 2018 earthquake. The objective of this study was to examine the soil susceptibility to the liquefaction phenomenon which might cause flash floods that resulted in the massive mudflows and soil dynamic effect in Palu City, to support the regional infrastructure planning and development. The soil susceptibility resulted from the dynamic effects was analyzed by combining the velocity amplification values obtained from microtremor measurements with the SPT derived from the site classification by using an ArcGIS framework.

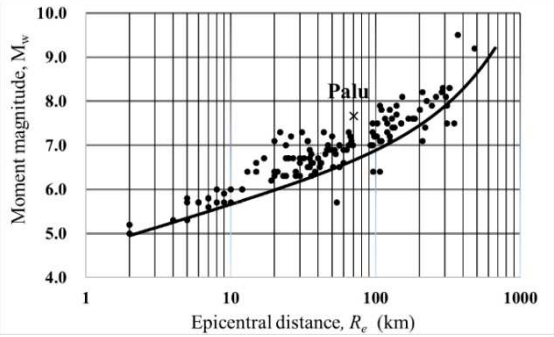


**Fig. 2** The maximum epicenter distance to liquefaction sites, $R_e$ and the moment Magnitude, $M_w$ (after (Ambraseys 1988))

## Geological Condition of Palu

### *Regional geological and tectonic setting*

Palu is located at the intersection of three main plates: Eurasian, Indian-Australian, and Pacific-Philippines plates, where the boundary of each plate is a relatively narrow deformation zone. The meeting point of the three plates is influenced by many other small plates, which makes Palu a complex area or later be known as a suture (Hall and Wilson 2000). The Sulawesi Suture was formed due to a plate collision between the Eurasian and Australian continents, which began in the early Miocene. Early Miocene rocks and younger ages were mostly recorded as magmatism and volcanoes, which then became an area of land and offshore sedimentation (Hamilton 1979). Central Sulawesi mostly consists of early Cretaceous metamorphic rocks. The underlying bases in this region consist of several metamorphic complexes overlapped by volcanic sediment deposits and magmatic intrusion, which vary in composition from gabbro and diorite to granodiorite and granite (Hamilton 1979).

The major geological structure in Central Sulawesi is the NNW-SSE oriented of Palu Koro fault (PKF) system, which stretches more than 300 km throughout Palu Bay to the city and connected to the North Sulawesi trench subduction zone. The geology of Palu City is composed of a structural system that is interpreted as a strike-slip feature, mostly with a concluded sinistral motion, as the Palu Koro fault system (Hall and Wilson 2000). The Palu Koro fault is a ground fault that is located far from the subduction zone with a strike-slip pattern and sinistral movement.

### *Geological condition of Palu*

The geology of the Palu area is dominated by sedimentary and volcanic deposits from the Cretaceous and Paleogene (**Fig. 3**). Palu contains five formations: Formation of the Alluvium and Coastal Deposits, Formation of the Celebes Molasse, Formation of Granite, Metamorphic Complex, and Formation of Tinombo. The Geological Survey of Indonesia investigated the formations in the 1970s by (Sukamto 1973).

The Palu City area is a quarter sedimentary expanse. Silty clay, silt, and alluvial sand and old river channel deposits were found along the Palu river at the lower elevations near the center of the valley. Young and old alluvium fan deposits are surficial sediments in the low relief hills, which extend on the west and east sides of the valley. Deposits of colluvium debris from gravel sand often occur at higher altitudes (Thein et al. 2014).

Balaroa morphology is approximately the same as Petobo, although Balaroa is located near the western hills where the slope is gentler. There is no irrigation channel in Balaroa, as opposed to another area affected by soil flow. The most likely factor of significant liquefaction in the region is influenced by the colluvial fan topographic, which is controlled by natural shallow groundwater (Faris et al. 2019). Petobo and Jono Oge are located on a gentle slope in the eastern hills. The morphology of the area is a colluvial deposition area originating from the hill.

## Research method

### *Horizontal to vertical spectrum ratio (HVSR) method*

Data resulted from the microtremor measurement was analyzed using the Horizontal to Vertical Spectral Ratio (HVSR) method. Then, a comparison was carried out between H (horizontal) and V (vertical) spectrum data. Introduced by (Nakamura 1989), the HVSR method was applied to estimate the resonance frequency and local sediment amplification factor of Microtremor data and also to estimate the soil susceptibility index (Nakamura 1997) and the building susceptibility index (Sato et al. 2008). The important parameters generated from the HVSR method are the resonance frequency and amplification factor. The HVSR method carried out for sediment data measurements should meet the criteria recommended by (SESAME 2004).

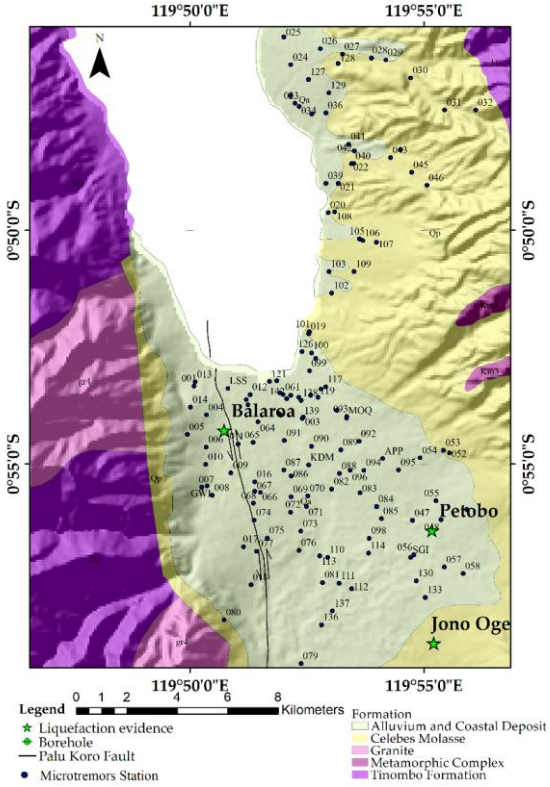


**Fig. 3** Geological map of Palu (Sukamto 1973)

By using the H/V ratio, the dominant frequency ($f_p$) and amplification factor ($A_p$) of the site can be determined. Nakamura also proposed the ground shear strain (GSS) to be used a means of determining the level of liquefaction (Nakamura 1997) by comparing the value of ground shear strain (GSS) and seismic susceptibility index ($K_g$) to determine the location of the soil movement in the 2018 liquefaction. The value of GSS and $K_g$ can be used to determine the location of vulnerable liquefaction points. A point with a higher $K_g$ value indicates higher liquefaction potential. The GSS values are determined from the soil structure strains, which can be defined as:

$$\gamma = K_g \alpha \tag{1}$$

where $\gamma$ = ground shear strain, $\alpha$ = peak ground acceleration at bedrock. The value of Kg can be used to verify the predicted liquefaction points by comparing them to the damage resulted from the 2018 earthquake. The $K_g$ value is obtained by squaring the HVSR spectrum with the peak value of the resonant frequency, which is determined by (Nakamura 2000) as:

$$K_g = \frac{A_g^2}{f_g} \tag{2}$$

where $K_g$ = the seismic susceptibility index, $A_g$ = amplification factor of the HVSR spectral peaks, and $f_g$ = natural frequency of the ground surface (Hz).

In this study, based on the Idriss and Boulanger 2008 method, the evidences of Balaroa liquefaction events was compared. The empirical method is more suitable for comparing the theory and field results of the liquefaction events. This method has been widely used by many researchers, such as (Mase et al. 2020; Jalil et al. 2020). The evaluation of the liquefaction is adopted from Idriss and Boulanger's (2008) method (Idriss and Boulanger 2008). The safety factor against liquefaction is determined by comparing the cyclic resistance ratio (CRR) and cyclic stress ratio (CSR), which is expressed as:

$$FS_{liq} = \frac{CRR_{M,\sigma'vc}}{CSR_{M,\sigma'vc}} \tag{3}$$

where $FS_{liq}$ = the safety factor against liquefaction. The values were predicted based on the N-SPT penetration resistance measured in various depths.

***Field investigation***

This paper uses the results of microtremor survey in 150 measurement stations carried out by (Thien 2015). The measuring instruments include the PIC, Portable Intelligent Collector, microtremor measurement device with three sensor components and a data recording unit. Microtremor was repeatedly recorded in 40.96 seconds (4,096 data in 100 Hz sampling) at each measured location, and 10.24 seconds data was selected from the viewpoint of less artificial noise (Sato et al. 2008). Then the selected data was transformed into Fourier before the ratio of the horizontal to vertical spectrum was calculated for each component of each measurement. Finally, the H/V spectrum ratio was derived as the average spectrum ratio (Nakamura 1989). The dominant frequency *f* and amplification factor *A* were obtained from the H/V spectral ratio. This procedure was performed in 1990. The data microtremor survey is presented in **Fig. 3** and the seven boreholes (BH) used for the analysis are shown in **Fig. 4**. They are located in the Balaroa village and Palu coastal area. The boreholes BH-1 and BH-2 was at a depth of 20 meters, and BH-3 to BH-7 was at a depth of 30 meters below the ground surface.

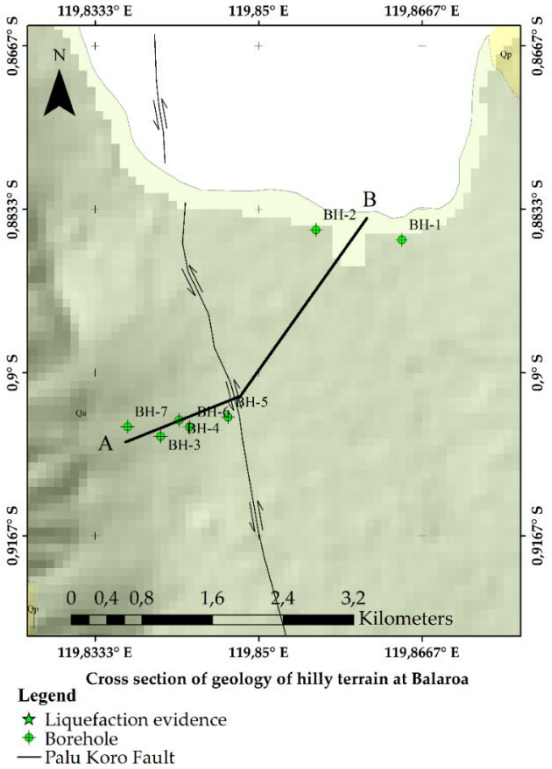


**Fig. 4** Locations of the Boreholes in Balaroa area

Figure 5 shows the ground slope plan-view from Balaroa village to the coastal area. The loose sand layer was found on the surface between 1 to 15 meters depth below the ground surface, whereas a relatively hard layer was found in the borehole BH-7. At a depth of 15 to 25 meters, the silty gravel layer was found with N-SPT value of 50. The average N-SPT value was higher than 50 at a depth of 25 to 30 meters, which indicates the existence of a

dense layer. The dominant sedimentary soil that stretches in the Palu basin consists of gravely sand, sandy silt, sand, silt, sand and gravel, and silty gravel.

The groundwater level (GWL) in the command area was between 0.3 and 10 meters below the ground surface. Groundwater at a depth of 0.3 m was found near the coast of the Palu City, while in the hills on the west of Balaroa, the ground water was found at a depth of10 m (**Fig. 5**). The boreholes BH-1 and BH-2 were located near the coastal area of Palu City, and BH-3 to BH-7 were on Balaroa gentle slope. A higher SPT value was found in BH-7 and BH-2, which were located on Balaroa steep slope and near to the coastal area, respectively. The soil resistance of BH-3, BH-4, BH-5, and BH-6 was relatively weak in comparison to BH-7 and BH-2. The variation of $(N_1)_{60}$ values is, as shown in **Fig. 5**.

The groundwater level in Palu Coast and Balaroa gentle slope was 0.3 meters and at a depth of 10 meters. respectively. The groundwater level in the Palu basin was shallow, with deposit soil layer containing loose sandy soil, confined aquifer, and low-level permeability (JICA 2019).

***Flow liquefaction analysis***

The flow liquefaction phenomenon may occur in either saturated loose sands, silts or very sensitive clays as it is associated with the contractive behavior of loose sand materials to become liquefaction. Such condition occurs during a strong earthquake (JICA 2019). A performance model was carried out by (Li and Ming 2000) to explain the liquefaction loading conditions. The simulations for undrained triaxial compression is started from anisotropic stress conditions. Laboratory test data and model that calculate the flow liquefaction and cyclic mobility illustrate the behavior of saturated loose sand, dense sand and undrained soils during the shear loading (monotonic and repetitive), as have been published by several researchers (P. K. Robertson 2010). In addition, by using SPT penetration resistance data, flow liquefaction can be predicted.

The corrected SPT blowcount $(N_1)_{60}$ shown in **Fig. 5** is employed to predict flow liquefaction. The procedure to evaluate the contractive state susceptibility of the soil to flow liquefaction based on the relationship between yield strength ratio and penetration resistance was proposed by (Olson et al. 2003) (**Fig. 9**). The yield strength ratio in **Fig. 9** presents the penetration resistance $(N_1)_{60}$ value that is limited to be less than 12 (Eq. 4). The boundary of the relationship between yield strength ratio and penetration resistance are describe as:

$$\frac{S_u\left(yield\right)}{\sigma_{v0}^{'}} = 0.205 + 0.0075\left[\left(N_1\right)_{60} \pm 0.04\right] \tag{4}$$

for $(N_1)_{60} \leq 12$

where $\frac{s_u\left(yield\right)}{\sigma_{v0}^{'}}$ is yield strength ratio, $(N_1)_{60}$ is penetration resistance.

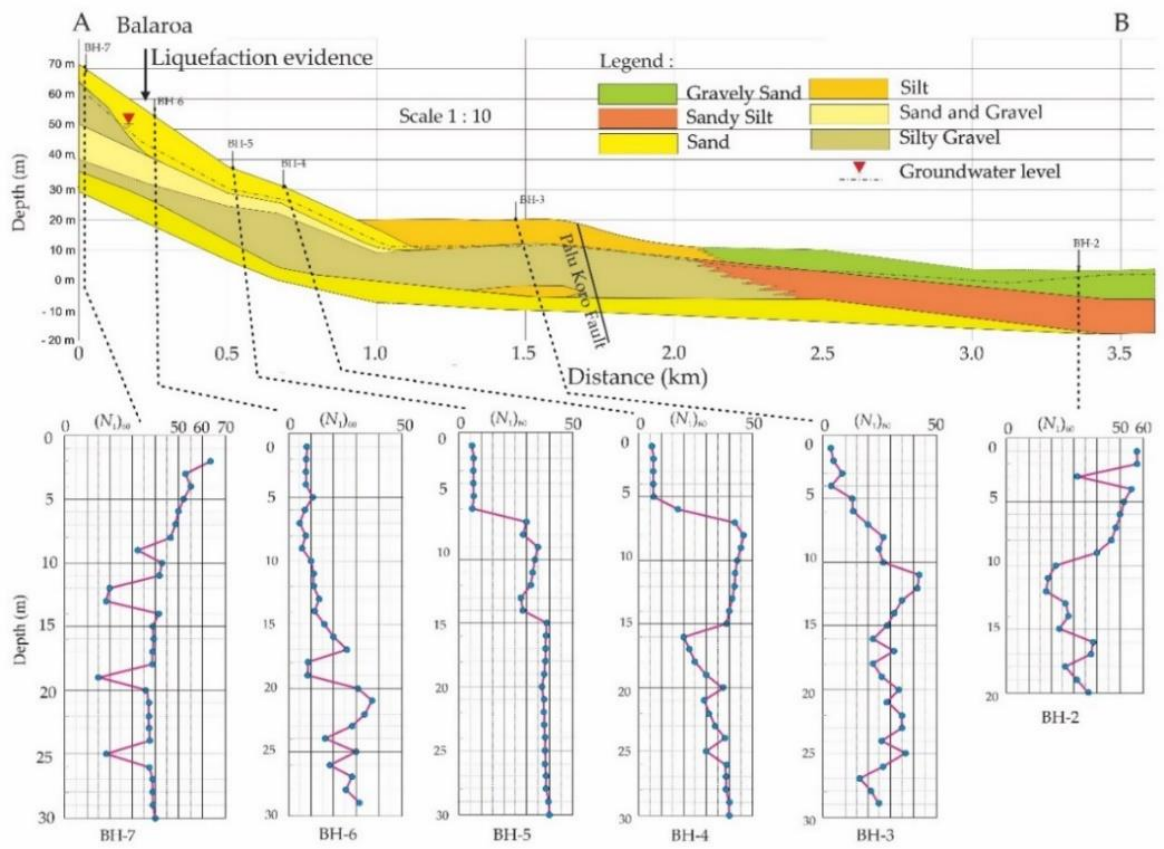


**Fig. 5** Balaroa soil profile based on A-B direction (modified (JICA 2019))

The liquefaction susceptibility to flow is highly dependent on the initial state of the soil. (Fear and Robertson 1995) proposed a susceptibility boundary relationship employing the concept of a critical state soil mechanics and laboratory test results. Based on the compatibility to the theory, laboratory test results, and field case history, (Fear and Robertson 1995) boundary is recommended for practices that describe whether a field is susceptible to a flow failure. This relationship is shown in **Fig. 10**. The recommended boundary relations can be expressed below:

$$\left(\sigma_{v0}^{'}\right)_{boundary} = 9.58\times10^{-4}\left[\left(N_1\right)_{60}\right]^{4.79} \tag{5}$$

***Flash flood caused mudflows***

Rapid land mass movement on gentle slopes is influenced by excess pore water pressure, when the earthquake shocks trigger the water pressure in the aquifer to emerge to the ground surface. The generation of pore water pressures on loss soil shear strength have changed into the wave of debris flow on the ground surface. Because, there are no data available to reveal the peak runoff during earthquake. This phenomenon is assumed to be a hypothesis that similar to flash floods due to high rainfall event in the river basins. Rainfall-induced landslides are one of the disasters that occur in complex areas of terrain, especially regions with heavy rainfall on a regular basis. Landslides can occur in a catchment area of unconsolidated soil prone to landslides, as well as flash floods that occur caused by the catchment area broken watersheds. In the case of landslides that take place in Balaroa, Petobo, and Jono Oge, they were caused by the breaking of the catchment area subsequent to Palu earthquake.

The gentle slope had fissures/cracks in the catchment area of Balaroa, Petobo and Jono Oge by 0.4 km2, 1.43 $km^2$, and 1.35 $km^2$, respectively (Mason et al. 2019). It is increasingly clear that flash flood is the major cause of infrastructure and casualties during earthquakes in gentle slopes. Rainfalls that's flows from catchment area into low level slope areas. The surface runoff referred to unit hydrograph and the methods of using unit hydrograph for designing the drainage system was applied. The empirical methods were performed to represent complex relationship between rainfall and peak surface runoff. The rational methods were conducted to analyze the runoff in relatively small catchment area. The runoff is expressed as:

$$Q = KiA \tag{6}$$

where $Q$ = the maximum runoff in ($cm^3/s$), $i$ = the designed mean intensity of rainfall (m/s), $A$ = area of catchment ($m^2$), $K$ = surface runoff coefficient, for slope $K$ is 1 (Geotechnical Control Office 1984).

Equation 6 is generally used to calculate the runoff, so the water spray from the aquifer layer can be assume as a runoff. Furthermore, i is the mean intensity of rainfall, which is assume to the velocity of water flowing on the sand as proposed by Darcy's law as follows:

$$v = \frac{\Delta h}{l} \tag{7}$$

By applying the Darcy equation, equation (6) becomes

$$Q = KvA \tag{8}$$

where $K$ = coefficient of surface runoff, v = velocity (m/sec), $\Delta h$ = different in height (cm), $k$ = coefficient of permeability (cm/s), $l$ = distance (cm).

## Results and discussion

### *Ground shear strain (GSS) and soil deformation*

The value of the ground shear strain is the parameter used to represent the soil strain in the event of earthquake. The higher the soil shear strain value, the more likely the surface sediment layer can stretch. These strains and shifts will cause deformations, such as soil fractures, landslides, and liquefaction (Nakamura 1989). Conversely, the smaller the GSS value, the lesser soil layer deformation is likely to occur. Ground shear-strain at the surface can be obtained by using Eq. 1. The PGA values at the bedrock are within the range 100-550 gals (Thein et al. 2014).

Figure 6 shows the distribution of ground shear-strain values depicted on the Digital Elevation Model (DEM) map of the command area. The sufficient value of the shear-strain was almost the same as the distribution of the $K_g$ value, where the moderate to high value was in the Palu valley area and in the directed of Palu Koro fault line. Soil layers will experience plastic conditions if the ground shear strain (GSS) values range from $1000\times10^{-6}$, and the ground shear strain (GSS) values ranges higher than $10{,}000\times10^{-6}$ (Ishihara 1996). Such soil condition is vulnerable to landslide and liquefaction whenever an earthquake occurs.

The values of GSS shows shallow sedimentary layers in Palu City, as presented in **Fig. 6**. The magnitude of GSS values ranged from $0.75 \times 10^{-4}$ to $2.56 \times 10^{-4}$. Within such range, the soil began to be elastic-plastic that the soil was easy to experience fractures and surface soil settlement. See Table 1 (Ishihara 1996). High ground shear strain values were in the southern, eastern, and western parts of Palu City, surrounding Balaroa and following the trail of the Palu Koro fault. These results tend to be similar to GSS (BMKG 2018).

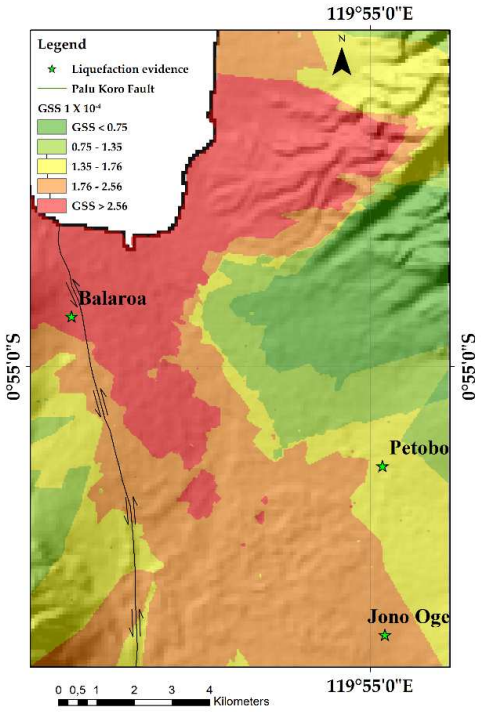


**Fig. 6** Ground shear strain (GSS) N-S direction at Palu City

Equation 2 is used to determine the value of the seismic susceptibility index ($K_g$). The Seismic susceptibility index is also related to geomorphological condition resonant frequency (See **Fig. 7**). A high value of seismic susceptibility indicates that the area consisted of alluvial material similar to the coastal area. Areas with high seismic susceptibility index ($K_g$) were found in the valley as well as coastal sediment areas. In hilly areas, it indicates a shallow seismic susceptibility index.

***The Liquefaction Analysis under the empirical methods***

The evaluation method of liquefaction using the N-SPT data is called the simplified procedure. It is a deterministic method using a seismic load by considering the Cyclic Stress Ratio (CSR). The ability of soil layer to resist liquefaction is expressed in the Cyclic Resistance Ratio (CRR). Liquefaction resistance of granular soils is also determined by using the CRR of the liquefaction potential assessment under the simplified shear stress technique (Idriss and Boulanger 2008).

**Table 1** Ground shear strain dependence of dynamic soil properties (Ishihara 1996)

| Size of GSS | $10^{-6}$ | $10^{-5}$ | $10^{-4}$ | $10^{-3}$ | $10^{-2}$ | $10^{-1}$ |
|---|---|---|---|---|---|---|
| Phenomena | Wave, vibration | | Crack, Settlement | | Landslide, Soil Compaction, Liquefaction | |
| Dynamic Properties | Elasticity | | Elasto-plasticity | | Collapse | |

Based on the geological characteristics, the investigation of the subsurface soil layer in the Balaroa areas shows that it was dominated by granular material. Sandy silt, silt and gravel, and dominant silt sand found in the first 20 m depth were with FC (fines content) in range 15-40%. This soil layer was followed by silt and sand in 30 m depth, wth FC ranging from 5-45%.

The soil classification was determined based on the average N-SPT of the top 30 m of the soil column. The procedure for calculating the average N-SPT follows the Indonesian Standards (SNI 03-1726-2019 2019). It indicates that soil in Balaroa is consisted of both medium soil (SD) and soft soil (SE) classifications. The characteristics of medium soil site (SD) class with N-SPT values 15 to 50 were found at BH-1, BH-2, BH-4, and BH-5 to BH-7 locations.

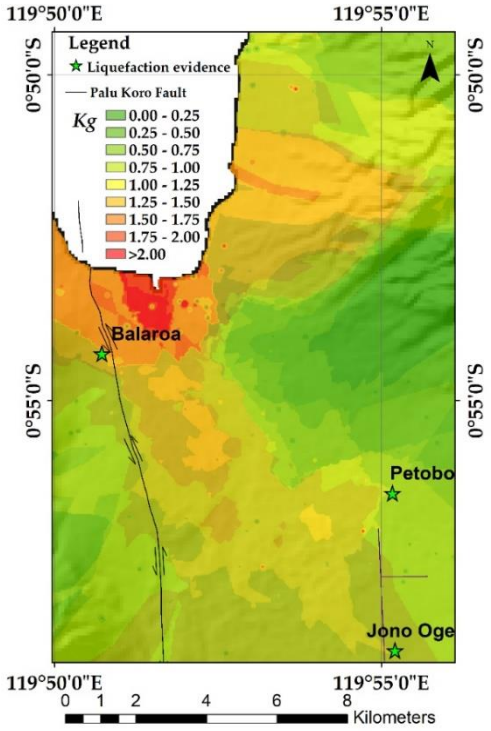


**Fig. 7** Seismic susceptibility index ($K_g$).

Meanwhile, the soft soil site class (SE) characteristics with N-SPT value ≤15 was found at BH-3 and BH-6 locations.

The Peak ground acceleration (PGA) on each borehole was determined based on the Indonesian National Standard or SNI 03-1726-2019. PGA was calculated by observing the specific site and considering the amplification factor, which includes the site coefficient ($F_{PGA}$) value. The maximum ground acceleration at the surface ($PGA_M$) is shown in Table 2.

The maximum PGA value was found in BH-1, which was located close to the coast, while the minimum PGA value was in the hilly area of BH-7. The areas near the coast indicated extreme ground motion due to its maximum soil density, which was stable against landslides. The gentle slope of the Balaroa hilly indicated maximum ground motion, in addition to the loose sand layer that enabled liquefaction to occur. The results of semi-empirical analyses are as shown in the liquefaction potential in **Fig. 8**. The analysis results prove that the liquefaction that occurred in 2018 could be predictable by using the microtremor seismic susceptibility index data ($K_g$).

**Table 2.** The value of $PGA_M$ on each borehole

| Borehole | GWL (m) | PGA (g) | $F_{PGA}$ | $PGA_M$ (g) |
|---|---|---|---|---|
| BH-1 | 0.8 | 0.823 | 1 | 0.823 |
| BH-2 | 0.3 | 0.797 | 1 | 0.797 |
| BH-3 | 3.2 | 0.732 | 1 | 0.732 |
| BH-4 | 2.1 | 0.738 | 1 | 0.738 |
| BH-5 | 0.55 | 0.755 | 1 | 0.755 |
| BH-6 | 6.0 | 0.742 | 1 | 0.742 |
| BH-7 | 10.0 | 0.722 | 1 | 0.722 |

The soil density parameters used in the analysis were the dry and wet soil unit weight of 17.0 kN/m$^3$ and 19.5 kN/m$^3$, respectively. The groundwater level influenced the calculation of total stress and not the effective vertical stress. The depth of the groundwater level is presented on Table 2. The results of the potential liquefaction calculation in BH-6 are presented in **Fig. 8**.

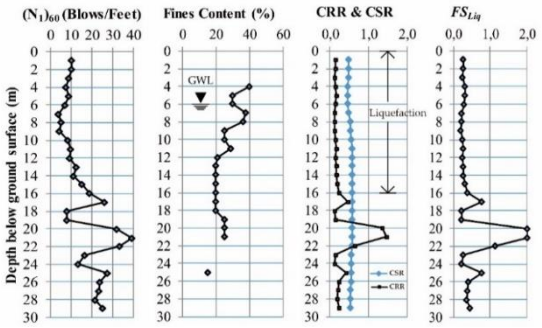


**Fig. 8** The example curve of $FS_{liq}$, CRR, and CSR at BH-6

Figure 8 shows that the depth of liquefaction was less than 16 meters below the ground surface. These locations experienced the liquefaction during the 2018 earthquake. The analysis of the potential liquefaction of all boreholes is shown on Table 3.

**Table 3.** Liquefaction Potential in each borehole

| Borehole | Safety Factor | Liquefaction Potential |
|---|---|---|
| BH-1 | $FS_{Liq}$ >1 | No Liquefaction |
| BH-2 | $FS_{Liq}$ >1 | No Liquefaction |
| BH-3 | $FS_{Liq}$ <1 | Liquefaction |
| BH-4 | $FS_{Liq}$ <1 | Liquefaction |
| BH-5 | $FS_{Liq}$ <1 | Liquefaction |
| BH-6 | $FS_{Liq}$ <1 | Liquefaction |
| BH-7 | $FS_{Liq}$ >1 | No Liquefaction |

***Flow liquefaction***

The penetration resistance plotted in **Fig. 9** is the values of $(N_1)_{60}$ which is limited to less than 12 based on the data in **Fig. 5**. The value of yield strength ratio as shown on Table 4 is generally referred to as residual strength and the denoted, $S_u$.

A study by (Ishihara 2019) showed that the calculation failure of the liquefaction flow was the back-calculation of the residual strength ratio based on the actual case of slide flow occurring in the Palu plains after the 2018 earthquake. The resulted $S_u$ values for Palu mainland ranges within 0.05 to 0.25 which are in accordance to the range values of residual strength ratio of 0.240 to 0.272 as shown on Table 4.

The nature of loose sand soil fabric with flow behavior can be evaluated based on the penetration resistance data (Fear and Robertson 1995). (Olson et al. 2003) conducted a static stability analysis to predict the migration of the soil particle with residual strength due to an earthquake. The SPT data based on the flow failure susceptibility relationships

**Table 4.** Yield strength ratio and $(N_1)_{60}$ value from **Fig. 9**.

| Borehole | $(N_1)_{60}$ | $\frac{s_u\,(yield)}{\sigma'_{v0}}$ | Liquefaction Potential |
|---|---|---|---|
| BH-1 | >12 | - | No liquefaction |
| BH-2 | >12 | - | No liquefaction |
| BH-3 | 3.91 | 0.240 | Flow liquefaction |
| BH-4 | 4.21 | 0.245 | Flow liquefaction |
| BH-5 | 6.43 | 0.260 | Flow liquefaction |
| BH-6 | 9.55 | 0.272 | Flow liquefaction |
| BH-7 | >12 | - | No liquefaction |

taken from the case history data proposed by (Fear and Robertson 1995) was used to carry out the susceptibility analysis of flow liquefaction. The susceptibility flow liquefaction in soil layer is identified by the soil contractive state (**Fig. 10**). The evaluation of liquefaction based on data $(N_1)_{60}$ and the vertical effective stress is plotted in **Fig. 10**. These plots show the layers of contractive soil and identify the flow failure. The plotting results as shown on Table 5 indicate that the region experiences flow failure, which is consistent with the 2018 liquefaction occurring in Palu City.

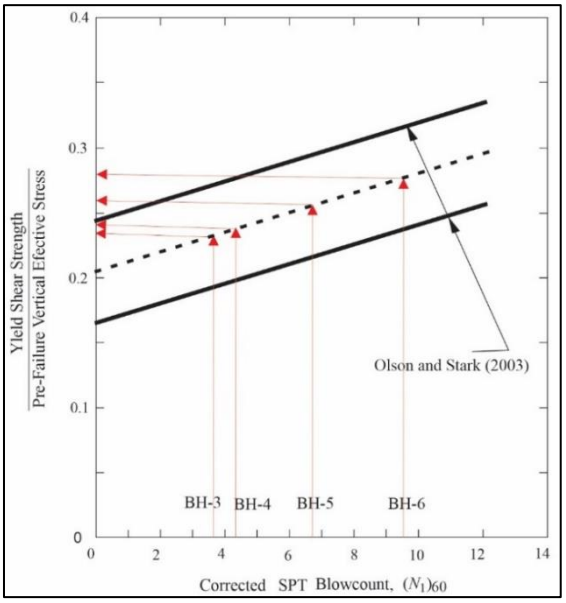


**Fig. 9** The corrected SPT blow count relationship to estimate liquefied strength ratios and for liquefaction flow failures, as proposed by (Olson et al. 2003). Red arrows indicate the BH-3, BH-4, BH-5, and BH-6 estimation

In addition, (Robertson I et al. 2019) also reported that based on the field monitoring, flow liquefaction taking place in the Balaroa, Petobo, and Jono Oge areas at the slope ground levels were 3.4%, 2%, and 1.4% respectively. Such softening soil moved to a distance up to 1,000 meters, 2,200 meters, and 3,900 meters for the area of Balaroa, Petobo, and Jono Oge, respectively. The soil movement was a distant trajectory that buried thousands of houses and other facilities in Balaroa, Petobo, and Jono Oge.

**Table 5.** Flow liquefaction susceptibility in each borehole

| Borehole | Depth (m) | $(N_1)_{60}$ | $\sigma'_{v0}$ (kN/m$^2$) | Liquefaction Potential |
|---|---|---|---|---|
| BH-1 | 1 | 28.90 | 15.54 | Dilative |
| BH-2 | 1 | >50 | 11.88 | Dilative |
| BH-3 | 4 | 3.91 | 62.15 | Contractive |
| BH-4 | 4 | 4.21 | 54.11 | Contractive |
| BH-5 | 6 | 6.43 | 62.16 | Contractive |
| BH-6 | 12 | 9.55 | 160.14 | Contractive |
| BH-7 | 1 | >50 | 17.00 | Dilative |

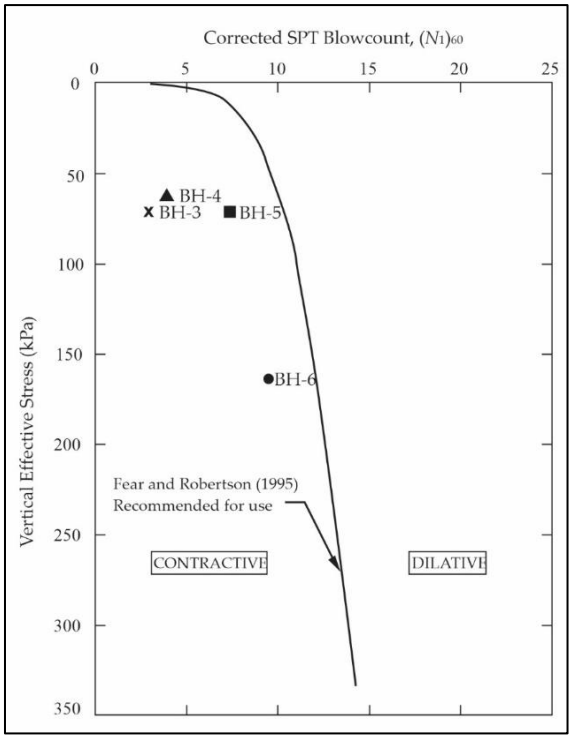


**Fig. 10** Separating relationships between contractive and dilative conditions by using the flow failure case histories and corrected SPT blowcount (Fear and Robertson 1995)

***A Phenomena of Flashflood like: the caused Mudflows***

Flow liquefaction occurrence in Palu City was similar to flash flood, which was the flow liquefaction as rapid flooding of water above the ground caused by a sudden burst of water from aquifer strip, or the release of retained water (e.g. the rupture of an impermeable confined aquifer) for a short period of time, usually within a few minutes to a few hours, a time scale that varies. This is what distinguishes it from fluvial flooding. The phenomenon of liquefaction in Palu City showed similar behavior to the flash floods event.

The uniqueness of the geological system in the region of Palu determines its hydro-morphological state, including that of the groundwater basin. On these sediment layers, lie Petobo, Balaroa, and Jono Oge that suffered a wide degree of liquefaction-induced-flow failure. This aquifer layer is the Palu groundwater basin, which has a very high average aquifer transmissivity value. The landslide event within the earthquake in Balaroa is illustrated in (**Fig. 11**).

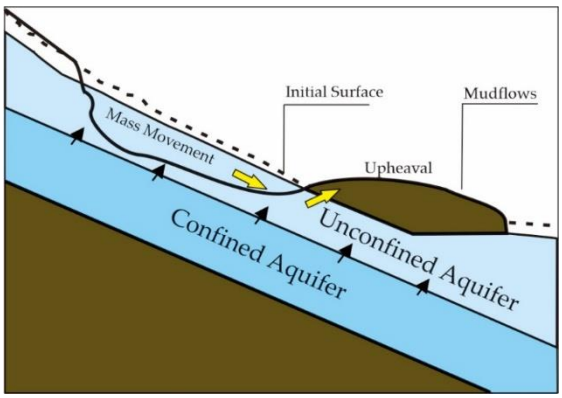


**Fig. 11** The illustration earthquake induced flow liquefaction in Balaroa

The groundwater level in Petobo area was shallow and also affected by the infiltration of the Gumbasa irrigation channel (**Fig. 12**). The soil layer was very saturated in addition to the presence of confined aquifer layer. The water flow in the channel enters the porous soil layer through the tear gap resulted from the earthquake shocks. In this condition, the soil turned into pulp and was carried away by the flash flood waves. The soil types in Petobo,

and Jono Oge are shown in **Figs. 14a** and **14b**, respectively. The soil layer was permeable and porous so that the sub-surface water pressed out through the gaps and raised the sediment by approximately 5 meters (JICA 2019). Such rapid change of stress in the soil made the effective vertical soil stress become zero and reached the maximum pore water pressure, thus, the soil layer induced large strain and liquify.

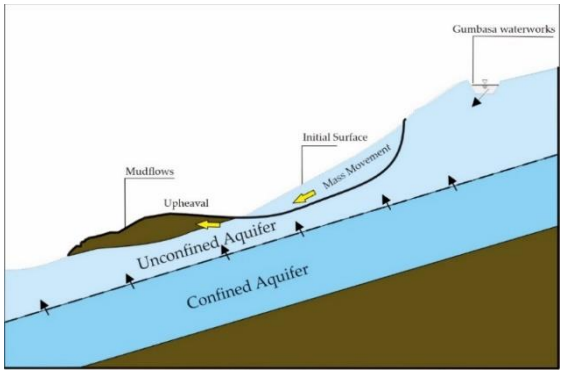


**Fig. 12** The ilustration of mudflows induced by earthquake in Petobo and Jono Oge

Movement of soil masses and rock debris down a slope or the rapid and gradual sinking of the ground surface in a dominant vertical direction are in response to the gravitational force. Ground movement velocity significantly affects the volume of land mass on the down slope. Soil mass movement velocity is strongly dependent on groundwater level fluctuation, dynamic viscosity coefficient, and sliding surface mass engineering properties (Naing et al. 2018). Considering the impacts and damages possibly caused by the mass movement, it is essential to predict its runout distance, velocity, moving volume, and coverage area (Fathani et al. 2017). The mass movement model was introduced by several researchers such as (Fathani et al. 2017; Syah et al. 2019). Small earthquakes of $M_w$ 4 can produce landslides, whereas the event $M_w$ > 7.5 usually create landslide of thousands of landslides on vulnerable slopes in an area of hundred square kilometers with millions of cubic volumes of loose material (Keefer 1994). (Keefer 1994) proposed a relationship between the magnitude of earthquakes and the historical number of landslides (**Fig. 13**). If **Fig. 13** is applied for the $M_w$ 7.5 landslide in Palu City with $M_w$ 7.5; it can be predicted that the volume of landslide material is $2.3\times10^8$ $m^3$, which is large volume of landslides that buried and swept away residential areas in Palu City. However, the volume of the landslide, triggered on September 28, 2018, $M_w$ 7.5 Palu earthquake, was estimated about $9.5\times10^6$ $m^3$. In all three locations, these volumes were calculated about 3 meter in height of debris and areas of at each site, the distribution of landslide were in Balaroa, Petobo, and Jono Oge.

By applying equations (6), (7) and (8), the results of the flash flood discharge and velocity can be obtained as shown on Table 6. The vertical permeability coefficient used in the calculations is based on the results of a field survey by (JICA 2019). Therefore, the peak runoff of water flash flood for Palu area could be calculated as the averaged value of the three locations from Table 6. The result is 11.31 $cm^3/s$.

The saturated mudflow material contained water that was equal to or higher than the Liquid Limit. Mudflow is a viscous liquid state and its criteria according to (Liu and Mason 2009) should be within the ratio of the average width and length of the soil mass movement, which ranges from 0.05 to 0.3. Meanwhile, the mudflow ratio in Palu city ranged from 0.2 to 0.4. However, there was some accordance between the criteria (Liu and Mason 2009) and the mudflow event in Palu region. As reported by (Meixler 2018), the shaking of the earthquake that resulted in loose material to become wave-like mudflows and move down the slope, was responsible for the massive damage in the Palu area.

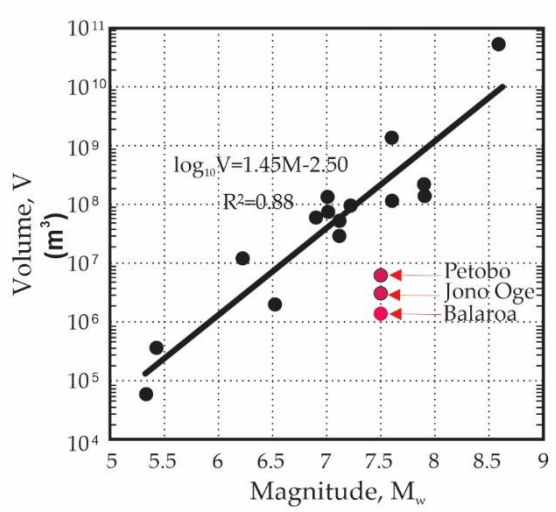


**Fig. 13** Earthquake magnitude versus total volume of material in landslides triggered by earthquake (modified (Keefer 1994))

The landslide that turned into mudflows in Balaroa was greatly influenced by a displacement of 3-5 meters of the total length of the 140 km of Palu Koro fault (Valkaniotis et al. 2018). The morphology mapping of landslide in Balaroa was impacted by secondary fault strand, which resulted in erosion; and in the case of Balaroa, the major mudflow damaged residential communities on the downstream of the main failure. The two landslide flows that occurred in Petobo and Jono Oge in the

Palu basin were within a large area of land deformation. However, the most significant land displacement scale was taken place in Jono Oge village (Hazarika et al. 2020).

**Table 6** The runoff of water effects flash flood in Palu area

| Vertical of permeability, $k$ (cm/s) | Different in height, $h$ (cm) | Distance, $l$ (cm) | Velocity, $v$ (cm/s) | $K$ | Catchment area, $A$ (cm²) | The runoff of water, $Q$ (cm³/s) | Location |
|---|---|---|---|---|---|---|---|
| $3.5 \times 10^{-3}$ | 1600 | $2.0 \times 10^{5}$ | $2.8 \times 10^{-5}$ | 1.0 | $0.40 \times 10^{6}$ | 11.20 | Balaroa |
| $3.5 \times 10^{-3}$ | 1600 | $7.0 \times 10^{5}$ | $8.0 \times 10^{-6}$ | 1.0 | $1.43 \times 10^{6}$ | 11.44 | Petobo |
| $3.5 \times 10^{-3}$ | 1600 | $6.7 \times 10^{5}$ | $8.4 \times 10^{-6}$ | 1.0 | $1.35 \times 10^{6}$ | 11.28 | Jono Oge |

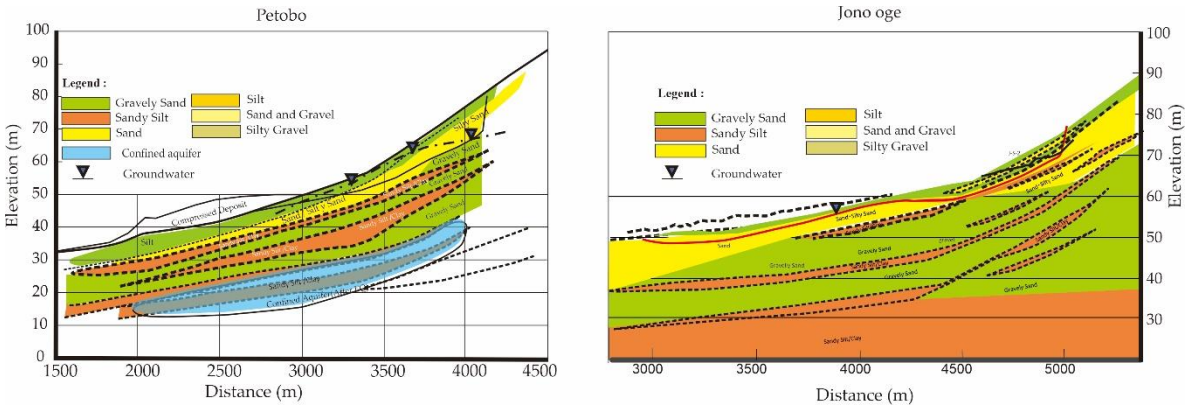


**Fig. 14** Geological profile proposed by (JICA 2019) after earthquake 2018, (**a**) cross-section in area mudflows of Petobo; (**b**) cross-section in area mudflows of Jono Oge

The displacement pattern of the area subsequent to the earthquake was able to be clearly defined. The rice cultivation area experienced displacement of > 5 m (Bradley 2019) was affected by the Gumbasa irrigation

channel and the rice planting scheme at the local location which raised the groundwater level. Based on the rational method approach, the average runoff peak at the Balaroa, Petobo and Jono Oge locations is presented on Table 6.

The limitations of this study in determining the water runoff caused by the flash floods during the Palu earthquake required further research. Groundwater depth position data was used to predict the emergence of runoff peaks which were assumed to be the same in all areas.

## Conclusions

This study presents a liquefaction analysis of the 7.5 $M_w$ earthquake that occurred in Palu, Indonesia, on September 28, 2018. The phenomenon of massive liquefaction led to mudflows in the Balaroa, Petobo, and Jono Oge areas. Microtremor and N-SPT seismic measurements were carried out to determine the soil susceptibility to the dynamic influence of the command area.

A liquefaction is controlled by the geological formation of alluvial deposits that are dominated by gravel sand and muddy sand. The Balaroa liquefaction was the only failure observed in the north to south side direction of the valley Palu. The displacement of the Balaroa slope triggered mudflow, which was most likely a secondary strand fault movement. With Petobo and Jono Oge areas being located on the western slope of the Gumbasa irrigation channel, the water flow on the channel also accelerated the emergence of mudflows through the ground fractures. It can be estimated that the average peak of water runoff causing the mudflow was approximately 11.31 $cm^3/s$.

Having shallow groundwater levels in the command area, the shaking of the 2018 earthquake affected the softening of the soil layer and consequently produced liquefaction in the Balaroa, Petobo, and Jono Oge regions.

Liquefaction events in Balaroa could be confirmed by using the semi-empirical analysis and susceptibility index approach from the microtremor survey. The result indicates that liquefaction can occur at a maximum depth of 16 meters below the ground level, as shown in **Fig. 8**.

Flow liquefaction in Balaroa, Petobo, and Jono Oge was strongly influenced by the presence of alluvial soil deposits and shallow groundwater levels prior to the earthquake shocks. Alluvial deposits are contractive behavior in areas with low density or penetration resistance $(N_1)_{60}$. Such contractive behavior is called the flow liquefaction.

### Abbreviations

BMKG; The Meteorological, Climatological, and Geophysical Agency; $M_w$: Moment Magnitude; LPI: Liquefaction potential index; N-S: North – South; NNW-SSE: North Northwest-South Southeast; $R_e$: Epicenter distance; H/V: Horizontal/vertical; $f_p$: Dominant frequency; $A_p$: Amplification factor; $S_u$: Undrained shear strain; SPT: Standard Penetration Test; N-SPT: Standard Penetration Test; PGA: Peak Ground Acceleration; CRR: Cyclic Resistance Ratio; CSR: Cyclic Stress Ratio; GWL: Groundwater level; $f$: Frequency; $A$: Amplitude. $FS_{Liq}$: Factor of Safety against liquefaction.

The datasets generated during and/or analysed during the current study are available in the
Jalil A, Fathani TF, Satyarno I, Wilopo W (2020): Liquefaction in Palu: The Cause of Massive Mudflows. figshare. Dataset. https://doi.org/10.6084/m9.figshare.13476729.v1

### Acknowledgments

The authors would like to express their gratitude for the support given by the Indonesian Endowment Fund for Education, as well as the Ministry of Research, Technology, and Higher Education.

### Author's contributions

"AJ performed the analysis data and experiments. TFF (promotor) supervised the work, partially conducted the data analysis as well as provided guidance in composing the liquefaction framework. IS (Co-Promotor) provided guidance in working with liquefaction and data analysis, WW (Co-Promotor) as geologist, helped with a guidance in the mechanism of geological hazard analysis procedure. All authors read and approved the final manuscript."

### Funding

The research was fully funded by Indonesian endowment fund for education.

**Competing interest:** The authors declare no conflict of interest.

Received: date; Accepted: date; Published: date

**References**


Ambraseys N N (1988) Engineering Seismology: Part II. Earthq Eng Struct D 17(1): 51–105. https://doi.org/10.1002/eqe.4290170102

Araujo W and Ledezma C (2020) Factors That Affect Liquefaction-Induced Lateral Spreading in Large Subduction Earthquakes. Appl Sci 10(18): 1-21. https://doi.org/10.3390/app10186503

BMKG (2018) Study of seismic parameters in the Palu region and surrounding areas. Available online: https://docplayer.info /110191815–Kajian–parameter–kerentanan-seismik-wilayah-kota-palu-dan-sekitar-nya. Accessed on 4 April 2020 (in Indonesia)

Bradley K, Mallick, R, Andikagumi H, Hubbard J, Meilianda E, Switzer A, Du N, Brocard G, Alfian D, Benazir, Feng G, Yun S H, Majewski J, Wei S, Hill E M (2019) Earthquake-triggered 2018 Palu Valley landslides enabled by wet rice cultivation. Nat Geosci 12(11): 935–939. https://doi.org/10.1038/s41561-019-0444-1

Faris F, Fathani T F, Wang F (2019) Report on the UNESCO Chair workshop on geoenvironmental disaster reduction 28th April -1st may, 2019, Palu-Jakarta, Indonesia. Geoenvironmental Disasters 6(12): 1-6. https://doi.org/10.1186/s40677-019-0129-5

Fathani T F, Legono D, Karnawati D (2017) A Numerical Model for the Analysis of Rapid Landslide Motion. Geotech Geol Eng 35(5): 2253–2268. https://doi.org/10.1007/s10706-017-0241-9

Fear C E, Robertson P K (1995) Estimating the undrained strength of sand: a theoretical framework. Can Geotech J 32(5): 859–870. https://doi.org/10.1139/t95-082

Geotechnical Control Office (1984) Geotechnical Manual for Slopes. 2nd Ed. Engineering Development Department Hongkong

Hall R, Wilson M E J (2000) Neogene sutures in eastern Indonesia. J Asian Earth Sci 18(6): 781–808. https://doi.org/10.1016/S1367-9120(00)00040-7

Hamilton W (1979) Tectonics of the Indonesian Region. Report 1078. Professional Paper. USGS Publications Warehouse. https://doi.org/10.3133/pp1078

Hazarika H, Rohit D, Pasha S M K, Maeda T, Irsyam M, Arsyad A, Nurdin S (2020) Large distance flow-slide at Jono-Oge due to the 2018 Sulawesi Earthquake, Indonesia. Soils Found. https://doi.org/10.1016/j.sandf.2020.10.007

Idriss I M, Boulanger R W (2008) *Soil Liquefaction During Earthquakes*. MNO-12, EERI Publications, United Stated of America, Earthquake. Engineering Research Institute, 2008, 1-264

Irsyam M, Hanifa N R, Djarwadi D, Sarsito D A, Widiyantoro S, Natawidjaja D, Meilano I, Rudyanto A, Hidayati S, Triyoso W, Faizal L, Sunarjito (2019) The Seismic Source and Hazard Map of Indonesia 2018 National Center for Earthquake Study (PUSGEN)

Ishihara K (1996) Soil behaviour in earthquake geotechnics. Oxford Engineering Science Series 45. Oxford: New York: Clarendon Press; Oxford University Press

Ishihara K (2019) Flow and Lateral Spreads of Liquefied ground following earthquakes. International conference on landslides and slope stability, Sept. 26-28, 2019, Bali, Indonesia

Iwasaki T, Tokida K, Tatsuoka F (1981) Soil liquefaction potential evaluation with use of the Simplified Procedure. Paper presented at the first International conference on recent advances in Geotechnical Earthquake Engineering and Soil Dynamic, St. Louis, Missouri April 26 – May 3, 1981

Jalil A, Fathani T F, Satyarno I, Wilopo W (2020) A study on the liquefaction potential in Banda Aceh City after the 2004 Sumatera Earthquake. Int J GEOMATE 18(65):147-155. https://doi.org/10.21660/2020.65.94557

JICA (2019) Project Report, the Project for Development of Regional Disaster Risk Resilience Plan in Central Sulawesi

Keefer, David K (1994) The importance of earthquake-induced landslides to long-term slope erosion and slope-failure hazards in seismically active regions. Geomorphology 10(1-4): 265– 284. https://doi.org/10.1016/0169-555X(94)90021-3

Li X S, Ming H Y (2000) Unified modeling of flow liquefaction and cyclic mobility. Soil Dyn Earthq Eng 19(5): 363-369. Doi.org/10.1016/S0267- 7261(00)00022-1

Liu, J G, Mason P J (2009) Essential Image Processing and GIS for Remotes Sensing. Wiley-BlackWell, London

Mase L Z, Likitlersuang S, Tobita T (2020) Verification of liquefaction potential during the strong earthquake at the border of Thailand Myanmar. J. Earthq. Eng. https://doi.org/10.1080/13632469.2020.1751346

Mason H B, Gallant A, Hutabarat D, Montgomery J, Reed A N, Wartman J, Irsyam M, Prakoso W, Djarwadi D, Harnanto D, Alatas I, Rahardjo P, Simatupang P, Kawanda A, Hanifa R (2019) The 28 September 2018 M7.5 Palu-Donggala, Indonesia Earthquake. GEER Association. https://doi.org/10.18118/g63376

Meixler E (2018) How liquefaction made flow like wave in Indonesia's earthquake disaster. TIME https://time.com/5413507/liquefaction-indonesia-earthquake-damage. Accessed on 23 September 2020

Naing M T, Fathani T F, Wilopo W (2018) Estimating the velocity of landslide movement using visco-plastic model in Jeruk Sub-village, Kulon Progo District, Yogyakarta, Indonesia. JCEF 4(3): 276-282. https://doi.org/10.22146/jcef.35097

Nakamura Y (1989) A Method for dynamic characteristics estimation of subsurface using microtremor on the ground surface. QR Railway Tech Res Inst 30(1):25–33

Nakamura Y (1997) Seismic vulnerability indices for ground and structures using microtremor. World Congress on Railway Research, Florence

Nakamura Y (2000) Clear Identification of Fundamental Idea of Nakamura's Technique and Its Applications. In: 12th World Conference on Earthquake Engineering, New Zealand, Paper No. 2656

Olson S M, Stark T D (2003) Yield strength ratio and liquefaction analysis of slopes and embankments. J Geotech Geoenvironmental Eng 129(8): 727-737. DOI: 10.1061/(ASCE)1090-0241(2003)129:8(727)

Robertson I, 35. Mulchandani H K, Achiari H, Esteban M, Mikami T, Nakamura R, Shibayama T, Stolle J, Takabatake (2019) Palu earthquake and tsunami, Sulawesi, Indonesia: Field Assessment Team 1 (FAT-1) Early Access Reconnaisssance Report (EARR). NHERI DesignSafe Project ID: PRJ-2128, 2019

Robertson P K (2010) Evaluation of flow liquefaction and liquefied strength using the Cone Penetration Test. J Geotech Geoenvironmental Eng 136(6): 842-853. https://doi.org/10.1061/(ASCE)GT.1943-5606.0000286

Sadly M (2018) Gempa Tektonik M=7,7 Kabupaten Donggala, Sulawesi Tengah pada Jumat 28 September 2018, Berpotensi Tsunami. BMKG. https://www.bmkg.go.id/press-release/?p= gempabumi-tektonik-m7-7-kabupaten-donggala-sulawesi-tengah-pada-hari-jumat-28-september-2018-berpotensi-tsunami&tag. Accessed on 22 January 2020 (in Indonesia).

Sato, Tsutomu, Nakamura Y, Saita J (2008) The change of the dynamic characteristics using microtremor. In World Conference on Earthquake Engineering. Beijing, China

SESAME. 2004. Guidelines for The Implementation of the H/V Spectral Ratio Technique on Ambient Vibrations Measurements, Processing and Interpretation. Project No. EVG1-CT-2000-00026 SESAME. Brussels, Belgium: European Commission – Research General Directorate

SNI 03-1726-2019 (2019) Earthquake Resistance Planning Ordinance for Building Structures and Non-Building. Badan Standardisasi Nasional. (in Indonesia)

Socquet A, Hollingsworth J, Pathier E, Bouchon M (2019) Evidence of supershear during the 2018 magnitude 7.5 Palu earthquake from space geodesy. Nat Geosci 12: 192–199. https://doi.org/10.1038/s41561-018-0296-0

Sukamto R (1973) Reconnaissance geological map of Palu area, Sulawesi. scale 1:250.000. Geological Survey of Indonesia, Bandung, Indonesia

Syah A, Fathani T F, Faris F (2019) A Numerical analysis of landslide movements considering the erosion and deposition along the flow path, JCEF 5(3): 187-200. DOI: https://doi.org/10.22146/jcef.43808

Thein P S, Pramumijoyo S, Brotopuspito K S, Kiyono J, Wilopo W, Furukawa A, Setianto A (2014) Estimation of seismic ground motion and shaking parameters based on microtremor measurements at Palu City, Central Sulawesi Province, Indonesia, World Academy of Science, Engineering and Technology International Journal of Geological and Environmental Engineering, 2014, 8, 308-319. doi.org/10.5281/zenodo.1092938

Thien P S (2015) Analysis of Strong Ground Motion Based on Microtremors, Boreholes and Trench Data in Palu City, Central Sulawesi Province, Indonesia. Dissertation, Universitas Gadjah Mada

Valkaniotis S, Ganas A, Tsironi V, Barberopoulou A (2018) A preliminary report on the M7.5 Palu earthquake co-seismic ruptures and landslides using image correlation techniques on optical satellite data. Zenodo 1-15. Doi: 10.5281/zenodo.1467128

Widyaningrum R (2012) Indonesian Geological Agency, Geological Investigation of Potential Liquefaction Engineering in Palu Central Sulawesi Province: Kementrian Energi dan Sumber Daya Mineral, Badan Geologi. Report No. 297/LAP-BGE.P2K/2012. (in Indonesia)

# Figures

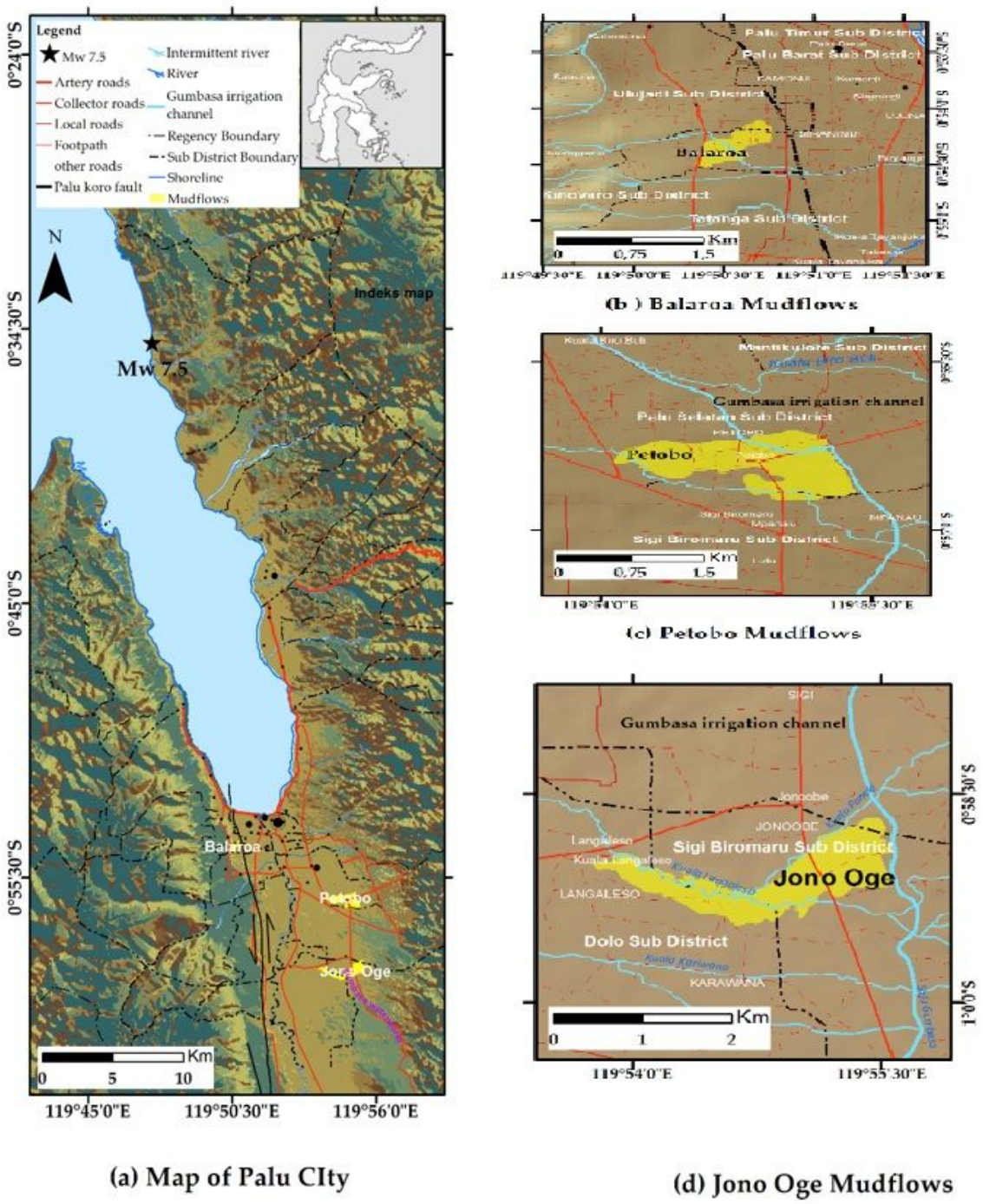


**Figure 1**

Liquefaction resulting mudflows in Palu City: (a) Map of Palu City, (b) Balaroa mudflows, (c) Petobo mudflows, and (d) Jono Oge mudflows

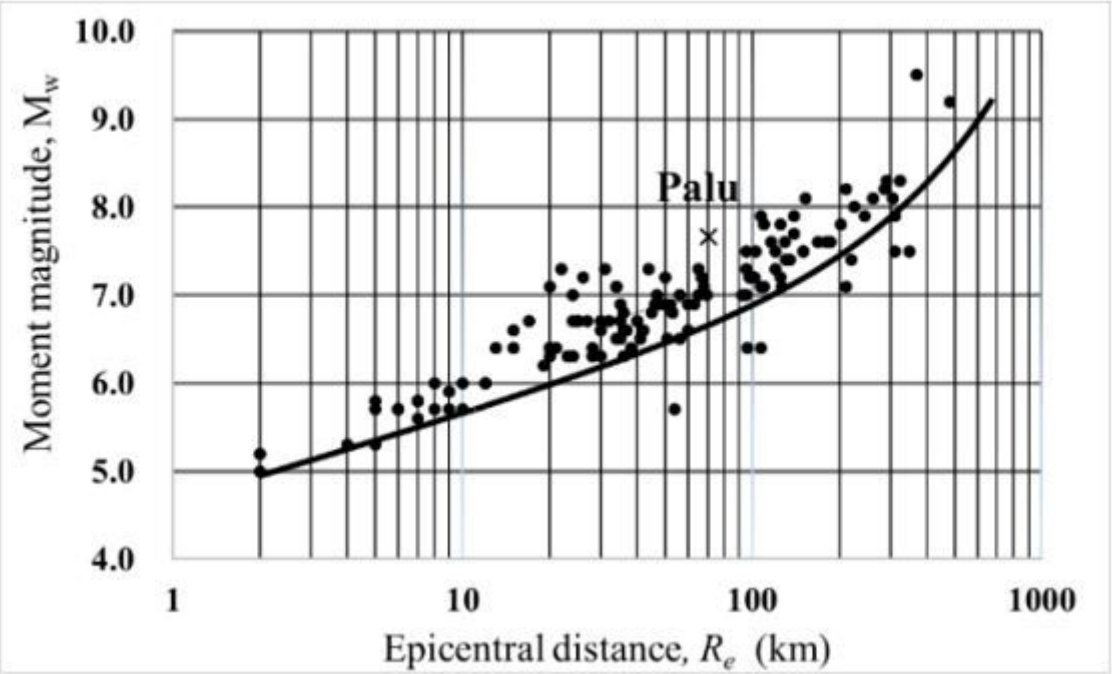


**Figure 2**

The maximum epicenter distance to liquefaction sites, Re and the moment Magnitude, Mw (after (Ambraseys 1988))

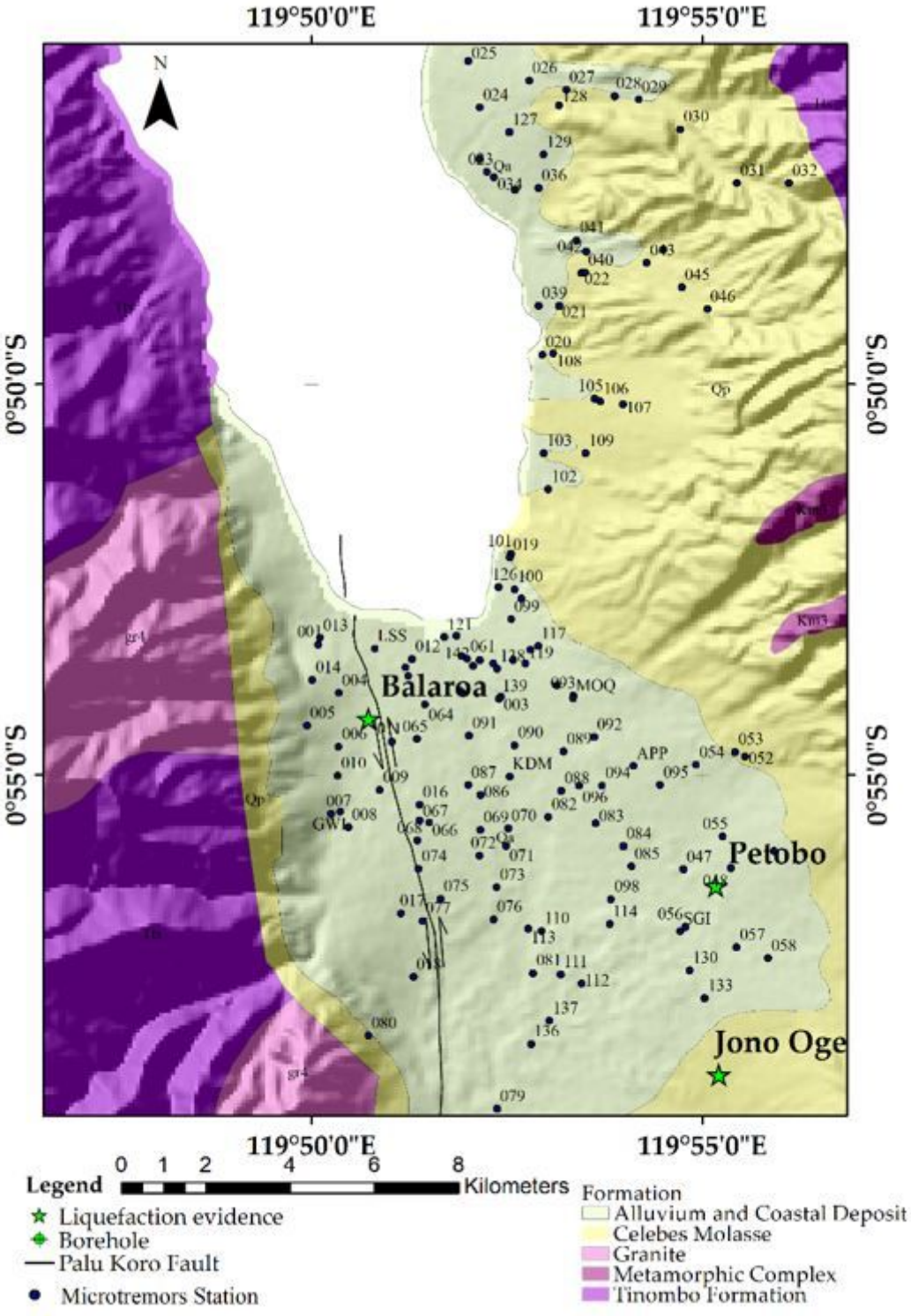


## Figure 3

Geological map of Palu (Sukamto 1973)

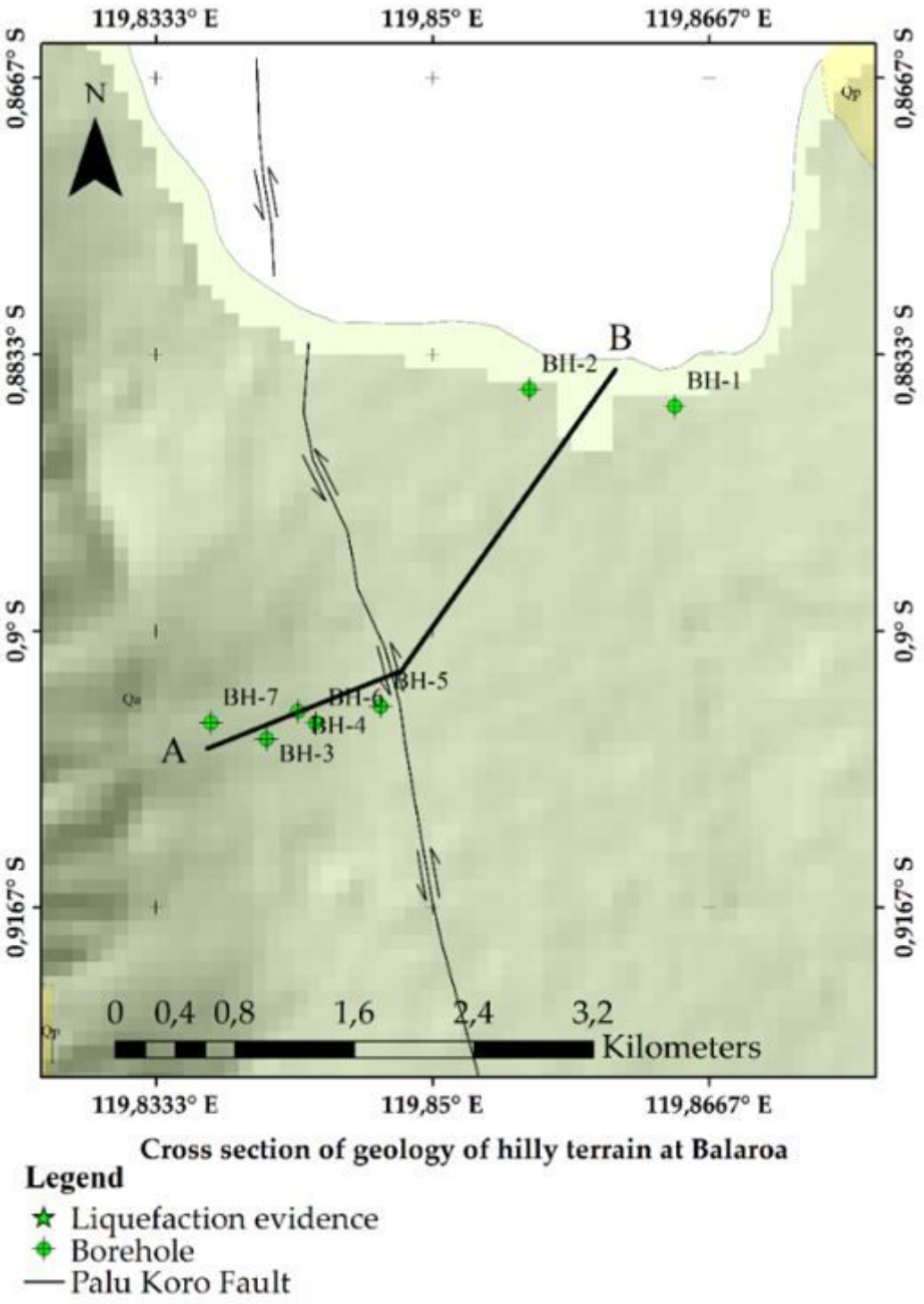


## Figure 4

Locations of the Boreholes in Balaroa area

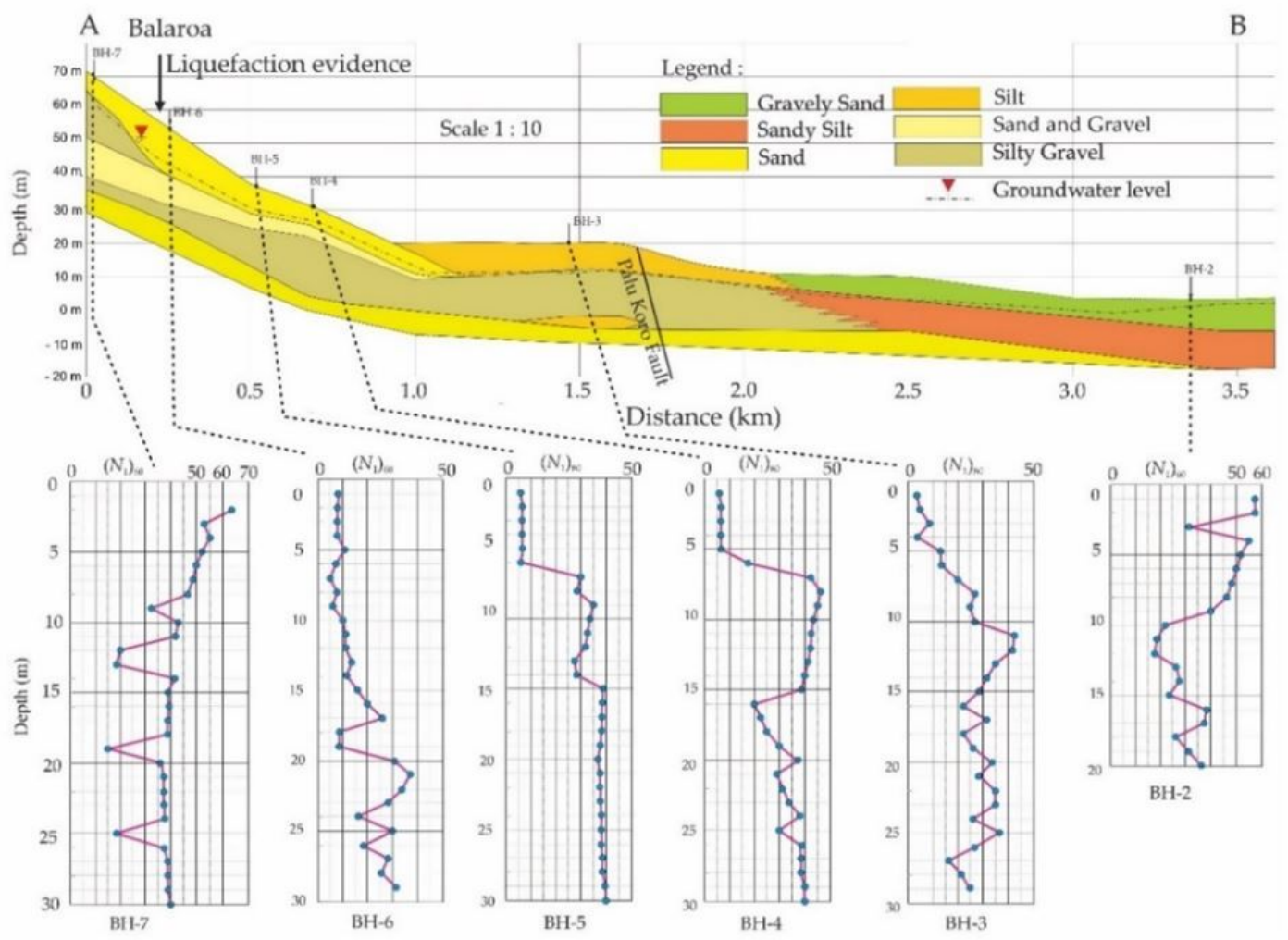


## Figure 5

Balaroa soil profile based on A-B direction (modified (JICA 2019))

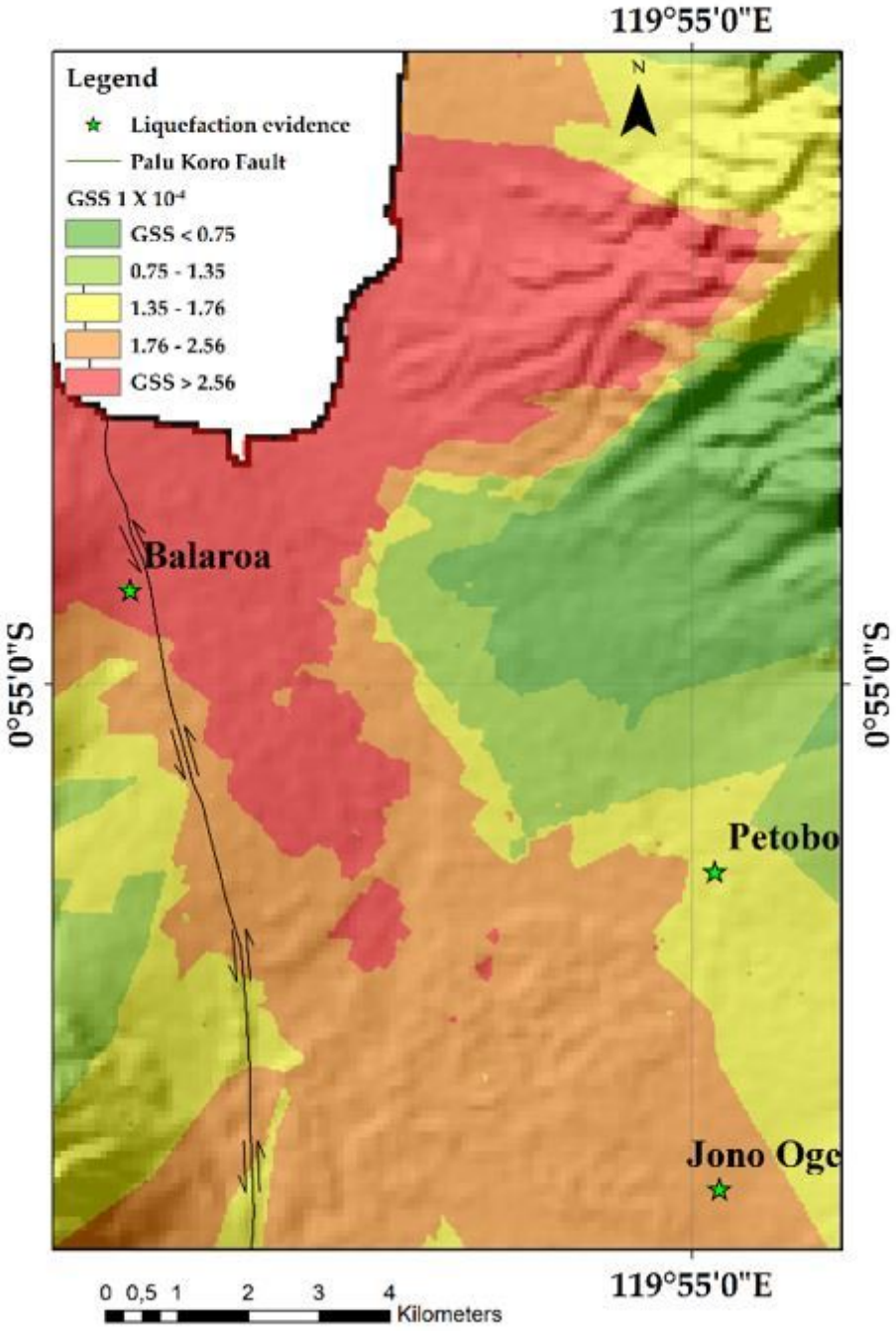


**Figure 6**

Ground shear strain (GSS) N-S direction at Palu City

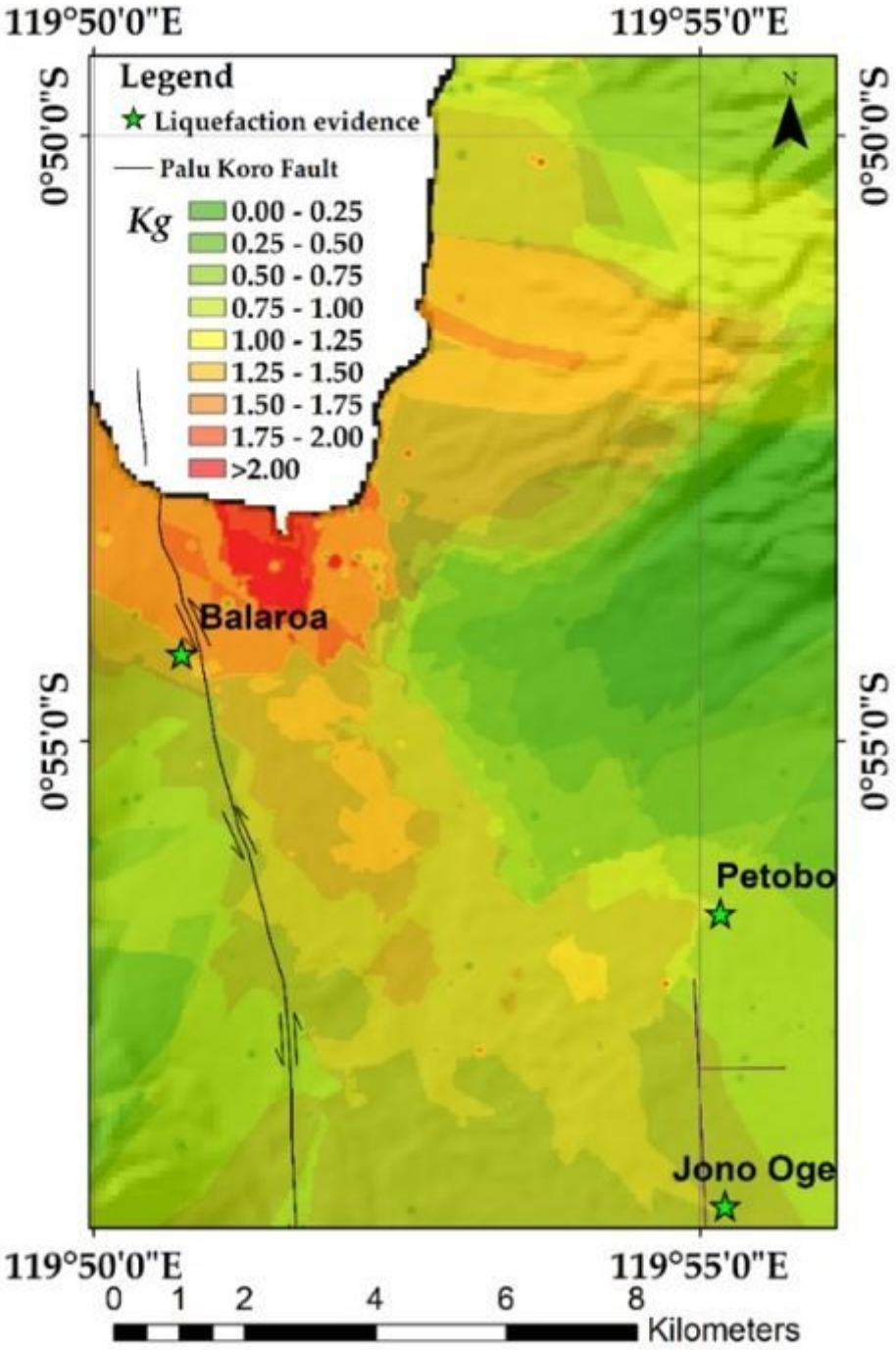


## Figure 7

Seismic susceptibility index (Kg).

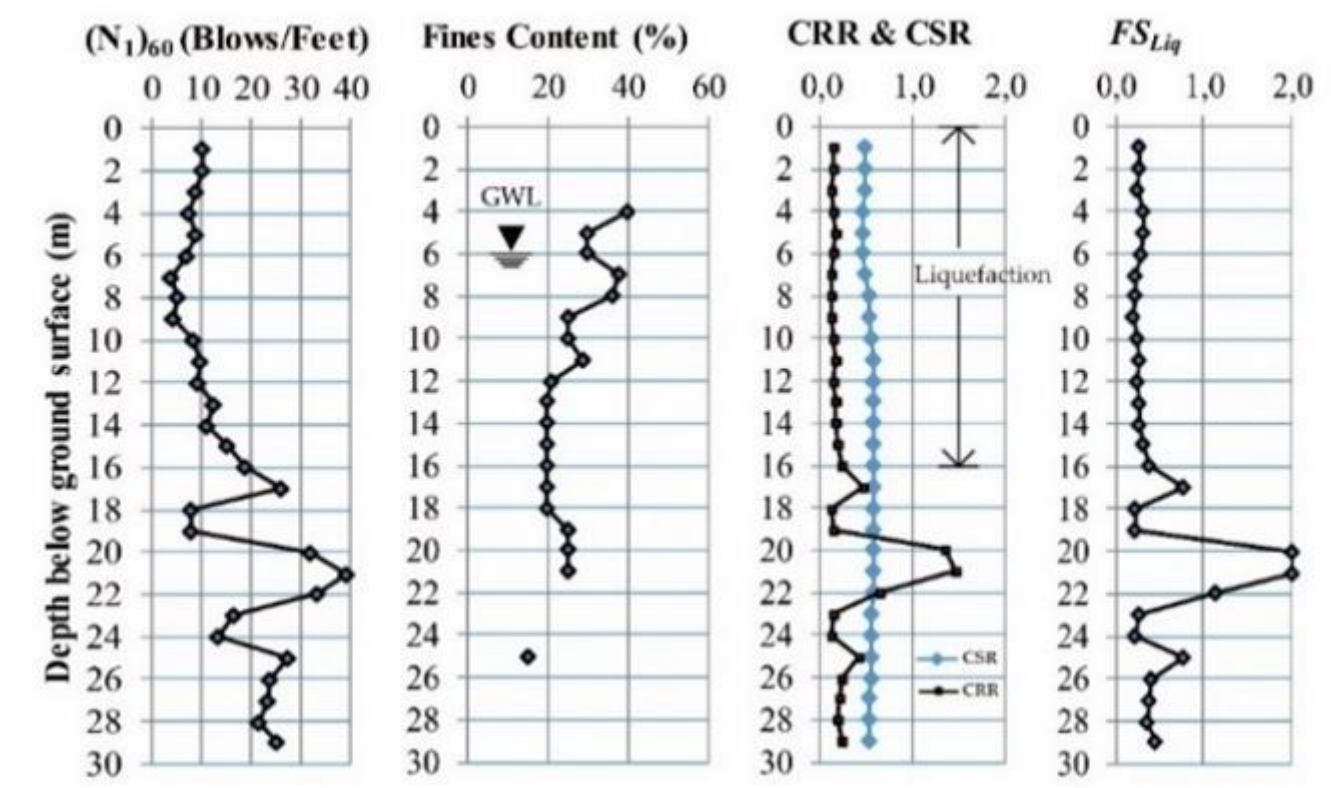


**Figure 8**

The example curve of FSliq, CRR, and CSR at BH-6

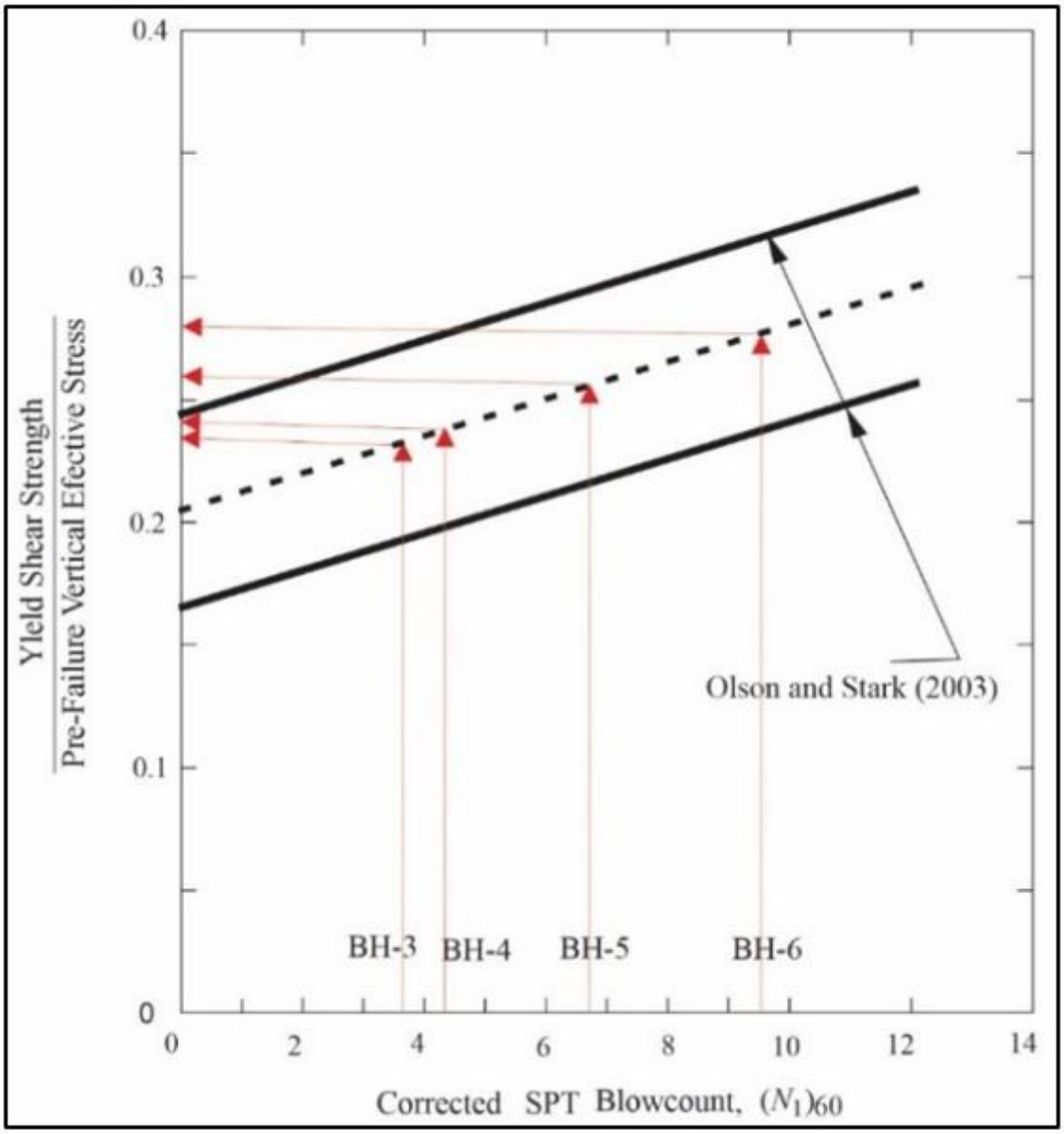


**Figure 9**

The corrected SPT blow count relationship to estimate liquefied strength ratios and for liquefaction flow failures, as proposed by (Olson et al. 2003). Red arrows indicate the BH-3, BH-4, BH-5, and BH-6 estimation

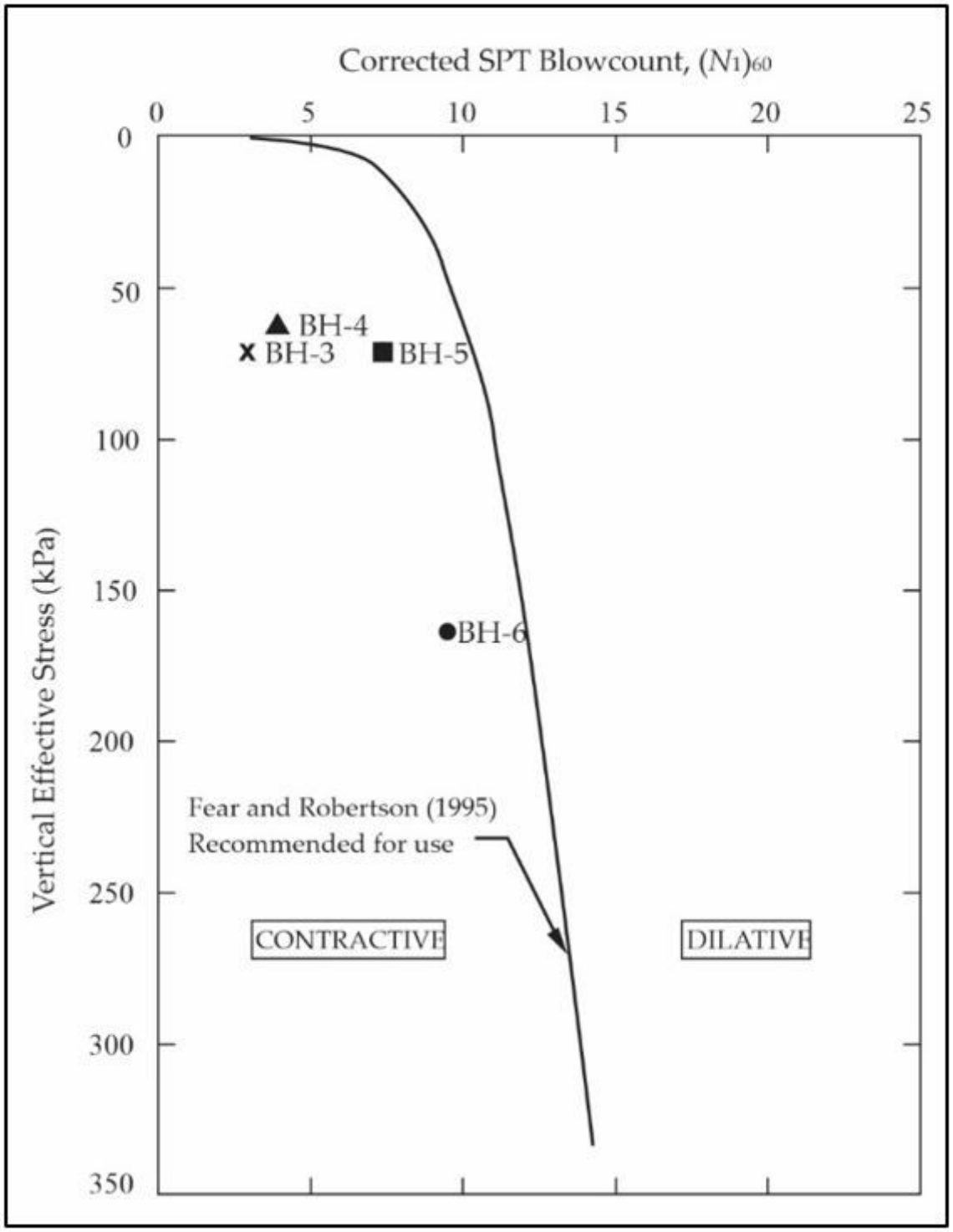


**Figure 10**

Separating relationships between contractive and dilative conditions by using the flow failure case histories and corrected SPT blowcount (Fear and Robertson 1995)

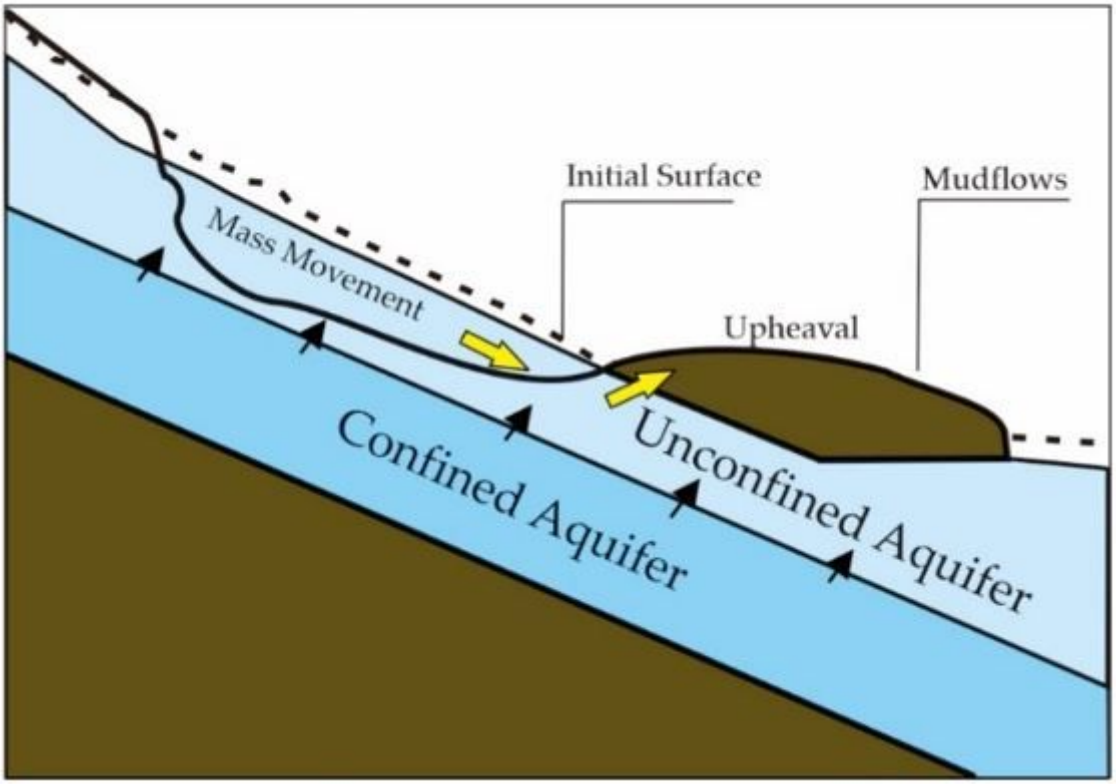


**Figure 11**

The illustration earthquake induced flow liquefaction in Balaroa

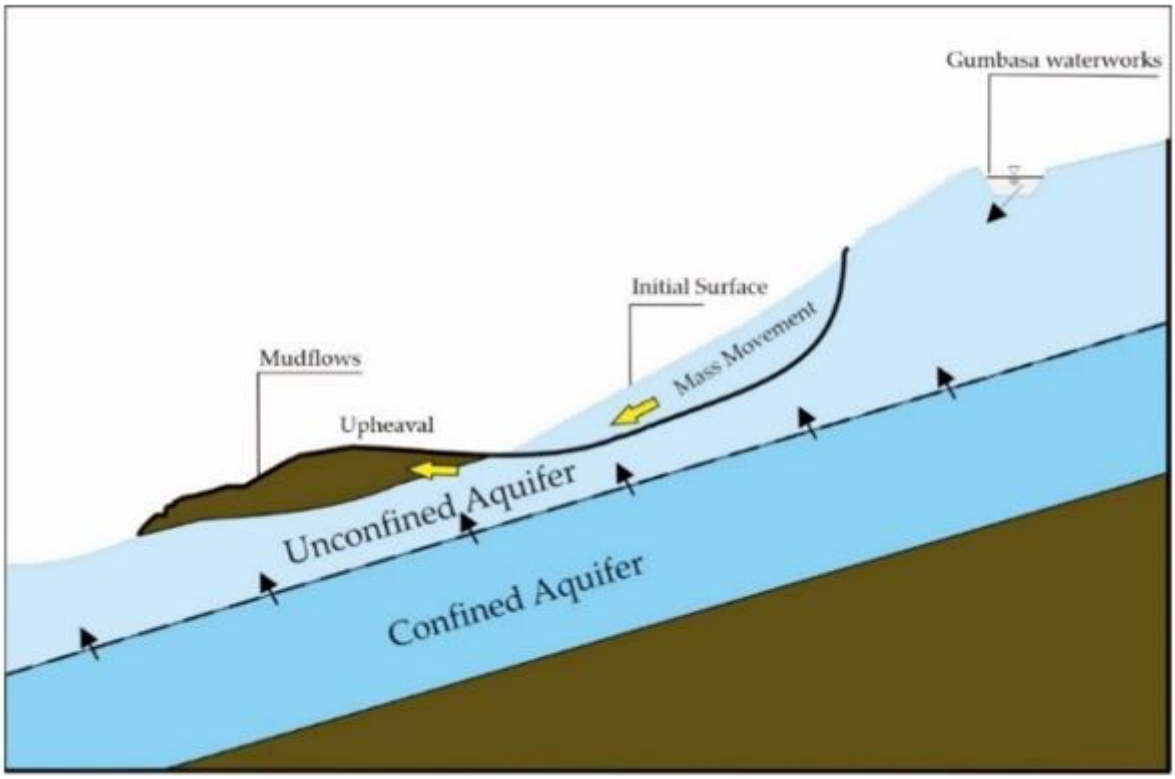

**Figure 12**

The ilustration of mudflows induced by earthquake in Petobo and Jono Oge

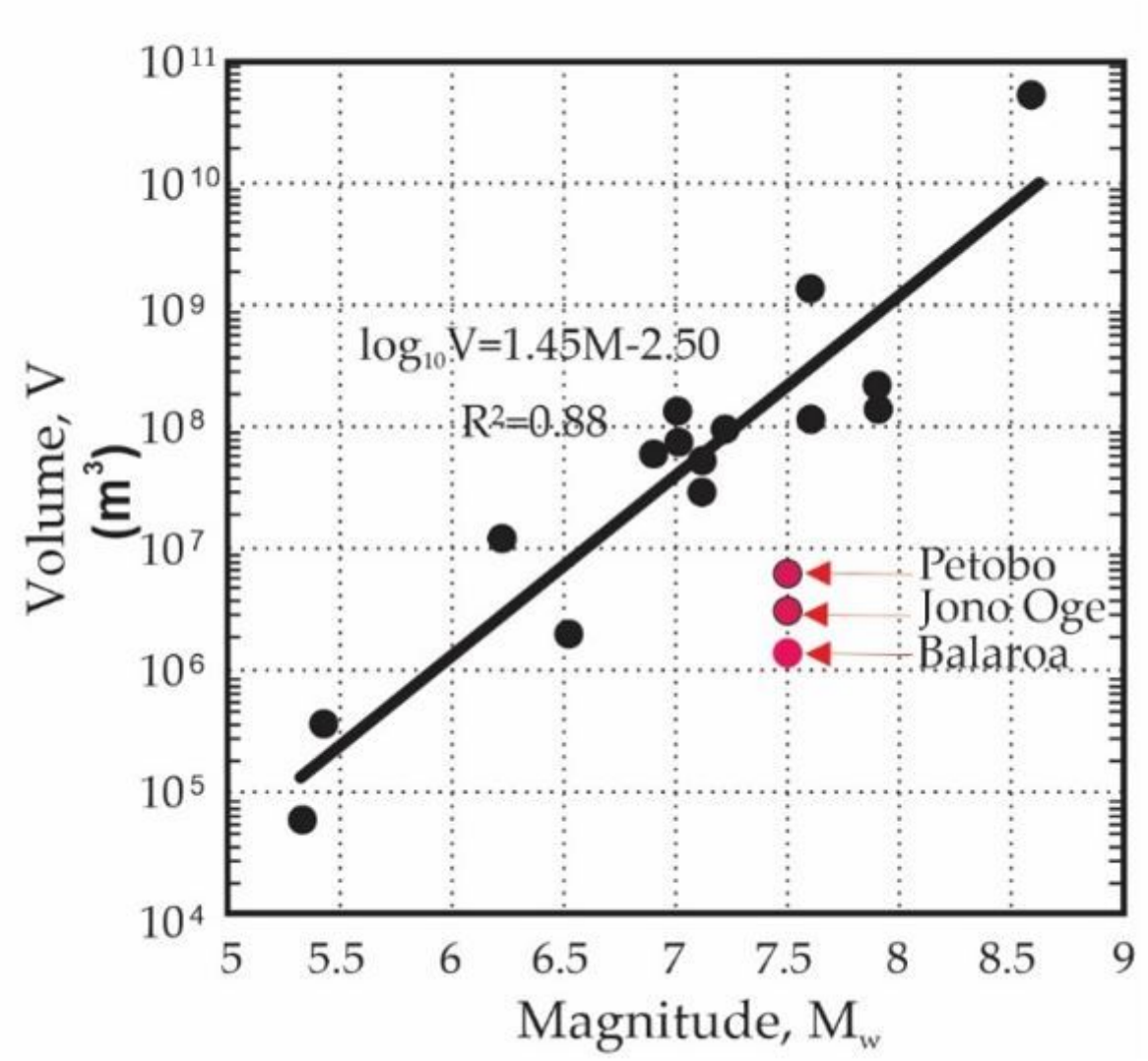


**Figure 13**

Earthquake magnitude versus total volume of material in landslides triggered by earthquake (modified (Keefer 1994))

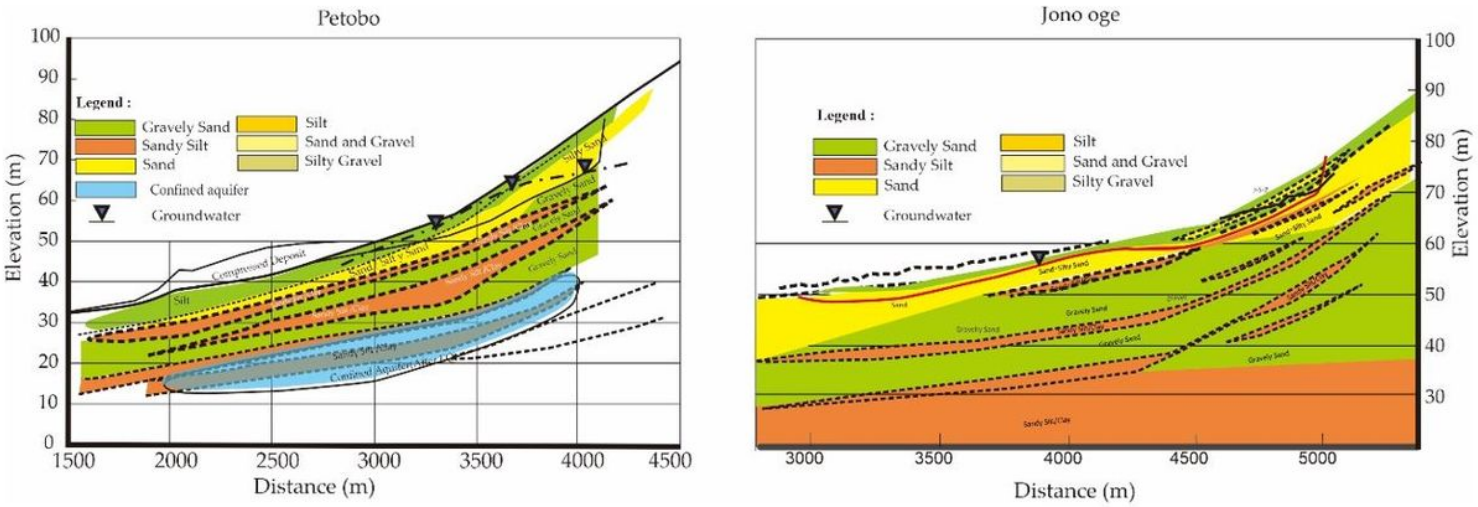


## Figure 14

Geological profile proposed by (JICA 2019) after earthquake 2018, (a) cross-section in area mudflows of Petobo; (b) cross-section in area mudflows of Jono Oge